Advancing Functional Genetics Through *Agrobacterium*-Mediated Insertional Mutagenesis and CRISPR/Cas9 in the Commensal and Pathogenic Yeast *Malassezia*

Giuseppe Ianiri, Gabriel Dagotto, Sheng Sun, and Joseph Heitman[1]
Department of Molecular Genetics and Microbiology, Duke University Medical Center, Durham, North Carolina 27710
ORCID ID: 0000-0002-3278-8678 (G.I.)

ABSTRACT *Malassezia* encompasses a monophyletic group of basidiomycetous yeasts naturally found on the skin of humans and other animals. *Malassezia* species have lost genes for lipid biosynthesis, and are therefore lipid-dependent and difficult to manipulate under laboratory conditions. In this study, we applied a recently-developed *Agrobacterium tumefaciens*-mediated transformation protocol to perform transfer (T)-DNA random insertional mutagenesis in *Malassezia furfur*. A total of 767 transformants were screened for sensitivity to 10 different stresses, and 19 mutants that exhibited a phenotype different from the wild type were further characterized. The majority of these strains had single T-DNA insertions, which were identified within open reading frames of genes, untranslated regions, and intergenic regions. Some T-DNA insertions generated chromosomal rearrangements while others could not be characterized. To validate the findings of our forward genetic screen, a novel clustered regularly interspaced short palindromic repeats (CRISPR)/Cas9 system was developed to generate targeted deletion mutants for two genes identified in the screen: *CDC55* and *PDR10*. This system is based on cotransformation of *M. furfur* mediated by *A. tumefaciens*, to deliver both a *CAS9*-gRNA construct that induces double-strand DNA breaks and a gene replacement allele that serves as a homology-directed repair template. Targeted deletion mutants for both *CDC55* and *PDR10* were readily generated with this method. This study demonstrates the feasibility and reliability of *A. tumefaciens*-mediated transformation to aid in the identification of gene functions in *M. furfur*, through both insertional mutagenesis and CRISPR/Cas9-mediated targeted gene deletion.

KEYWORDS *Malassezia furfur*; insertional mutagenesis; CRISPR/Cas9; protein phosphatase 2A; pleiotropic drug resistance

THE genus *Malassezia* is a lipophilic, monophyletic group of basidiomycetous yeasts that colonize sebaceous skin sites and represents > 90% of the skin mycobiome (Findley *et al.* 2013; Wu *et al.* 2015; Byrd *et al.* 2018). In addition to their ubiquitous presence on the skin of humans and animals, recent data support the hypothesis that *Malassezia* fungi are much more widespread than previously thought. Metagenomic studies have revealed the presence of *Malassezia* DNA in a number of unexpected areas, such as in association with corals and sea sponges in the ocean (Amend *et al.* 2019).

Malassezia are highly divergent from other fungi that are commonly found on the skin, such as *Candida* species and the dermatophytes, and there are currently 18 species within the *Malassezia* genus. *Malassezia* species belong to the Ustilaginomycotina subphylum, which includes the plant pathogens *Ustilago*, *Sporisorium*, and *Tilletia*, and are highly divergent from other basidiomycetous fungi that infect humans, such as *Cryptococcus neoformans*. A defining characteristic of the *Malassezia* genus is the lack of a fatty acid synthase, a Δ^9 desaturase, and a $\Delta^{2,3}$ enoyl-CoA isomerase, making them lipid-dependent, and difficult to study and manipulate under laboratory conditions. Recent classifications have revealed that *Malassezia* represents a sister group to the blast yeast-

doi: https://doi.org/10.1534/genetics.119.302329
Manuscript received May 13, 2019; accepted for publication June 22, 2019; published Early Online June 26, 2019.
Supplemental material available at FigShare: https://doi.org/10.25386/genetics.8309342.
[1]Corresponding author: Department of Molecular Genetics and Microbiology, Duke University Medical Center, Box 3546, 322 Carl Bldg., Research Drive, Durham, NC 27710. E-mail: heitm001@duke.edu

like fungi *Moniliella* (Wang *et al.* 2014, 2015), which also includes species reported to be pathogenic on human and animal skin (McKenzie *et al.* 1984; Pawar *et al.* 2002).

In the last decade, there has been increasing scientific interest in *Malassezia*, with several sequencing projects aimed at defining genomic features and gene content for 15 broadly recognized *Malassezia* species. All haploid *Malassezia* species have small genomes compared to other phylogenetically related fungi (7–9 Mb compared to ~20 Mb), with the exception of *Malassezia furfur* hybrid species whose genomes are twice the size of other *Malassezia* species. Genome analyses have revealed intriguing features, such as (1) loss of the RNA interference pathway components; (2) evidence of horizontal gene transfer events from bacteria; (3) the presence of genes unique to *Malassezia*; and (4) expansion of secreted protein, lipase, and protease gene families that encode products predicted to breakdown lipids and proteins important for growth, and host–microbe interactions (Xu *et al.* 2007; Gioti *et al.* 2013; Triana *et al.* 2015; Wu *et al.* 2015; Park *et al.* 2017; Zhu *et al.* 2017; Kim *et al.* 2018; Lorch *et al.* 2018; Cho *et al.* 2019; Morand *et al.* 2019). It is likely that the genomes of *Malassezia* species have reduced over time concomitantly with their evolution as a commensal organism and adaptation to the skin (Wu *et al.* 2015). There are other cases in which fungal genome reduction correlates with niche specialization, with the most remarkable examples being the obligate *Pneumocystis* species, with genomes of ~7–8 Mb (Ma *et al.* 2016), and *Microsporidia* species, with genomes as small as 2.9 Mb (Cuomo *et al.* 2012).

Aside from their commensal lifestyle, *Malassezia* fungi have been associated with several skin disorders, including pityriasis versicolor, dandruff, severe atopic dermatitis in humans, and otitis in dogs (Gaitanis *et al.* 2012; Wu *et al.* 2015). However, the exact role of *Malassezia* in these clinical conditions has been controversial, with recent studies even hypothesizing a protective role of *M. globosa* against *Staphylococcus aureus*, a bacterium that is associated with severe atopic dermatitis (Ianiri *et al.* 2018; Li *et al.* 2018). The lack of knowledge regarding *Malassezia* functions within the skin mycobiome is due, in part, to the dearth of experimental systems for studying *Malassezia*–host interactions; current knowledge is based solely on *in vitro* experiments with isolated host cells (Watanabe *et al.* 2001; Ishibashi *et al.* 2006; Donnarumma *et al.* 2014; Glatz *et al.* 2015; Sparber and LeibundGut-Landmann 2017). Recently, two groundbreaking studies reported novel experimental murine models for studying *Malassezia* interactions with the skin and intestinal mucosa (Limon *et al.* 2019; Sparber *et al.* 2019), and their importance has been highlighted in two commentaries (Dawson 2019; Wrighton 2019).

Although these models represent an important advancement of our understanding of the mechanisms of host responses to *Malassezia*, a lack of technologies for functional genetic studies has hampered the identification and characterization of the fungal components that promote inflammation, and induce host responses. We developed a transformation system based on *Agrobacterium tumefaciens*-mediated transformation (AtMT) that is effective for both insertional and targeted mutagenesis, and enabled the first genetic manipulation of *M. furfur* and *M. sympodialis* (Ianiri *et al.* 2016, 2017a). Subsequently, *M. pachydermatis* has also been transformed (Celis *et al.* 2017).

CRISPR (clustered regularly interspaced short palindromic repeats)/Cas9 was originally discovered as a mechanism of adaptive bacterial immunity (Jinek *et al.* 2012). The CRISPR/Cas9 system has been modified for use in other organisms and, at present, represents a revolutionary technology that has allowed gene editing in a number of cell types, including fungi (Shi *et al.* 2017; Adli 2018). The system consists of two elements, a specific endonuclease (Cas9) and a guide RNA (gRNA), that form a complex that catalyzes double-strand breaks (DSBs) at a specific DNA site flanking a protospacer adjacent motif (PAM) sequence of the host genome. After the DSB is generated, the DNA is repaired either through non-homologous end joining or through homology-directed repair (HDR) when donor DNA is provided (Shi *et al.* 2017).

The present study is divided into two sections. In the first, we built upon the previously developed AtMT technology to perform the first transfer (T)-DNA-mediated genetic screen in *M. furfur*. The aim was to generate a library of random insertional mutants, select for mutants with a phenotype of interest, and characterize insertion sites within the *M. furfur* genome to infer the function of genes involved in physiological and clinical processes of interest. In the second part of this study, we developed the first efficient, transient CRISPR/Cas9 mutagenesis system for *Malassezia*, and successfully generated targeted deletion mutants of two genes identified in the forward screen: *CDC55*, which encodes a subunit of protein phosphatase 2A (PP2A), and *PDR10*, which encodes an ATP-binding cassette (ABC) transporter predicted to be involved in pleiotropic drug resistance. While validating the effectiveness of the T-DNA insertional mutagenesis for gene function studies, this novel CRISPR/Cas9 method enabled us to overcome issues related to the reduced rate of homologous recombination (HR) observed in *M. furfur*, and we expect that this technology will facilitate future molecular research on *Malassezia* fungi.

Materials and Methods

Strains and culture conditions

The haploid *M. furfur* strain CBS14141 (previously known as JPLK23) was used as the wild-type (WT) strain for transformation experiments. This strain was maintained on modified Dixon's media (mDixon) [mycological peptone (10 g/liter), malt extract (36 g/liter), glycerol (2 ml/liter), tween 60 (10 ml/liter), desiccated ox-bile (10 g/liter), and agar (20 g/liter) for solid media]. Transformants were maintained on mDixon supplemented with the antifungal agents nourseothricin (NAT) or G418 (NEO).

Forward genetics screen in M. furfur

Insertional mutagenesis was performed through AtMT using *A. tumefaciens* strain EHA105 engineered with the binary vectors pAIM2 or pAIM6, which contain *NAT* and *NEO* resistance markers under the control of the *M. sympodialis ACT1* promoter and terminator, respectively (Ianiri *et al.* 2016). Initially, transformations were performed using previously developed methods (Ianiri *et al.* 2016; Celis *et al.* 2017). Selected transformants were colony purified on selective media and arrayed in 96-well plates containing 100 μl of mDixon + NAT or mDixon + NEO for *in vitro* assays and long-term storage.

For the primary screen, a 1.5-μl aliquot of cellular suspension of transformants was spotted on mDixon agar containing the following chemicals: Congo red (0.5%), sodium chloride (NaCl, 1 M), sodium dodecyl sulfate (SDS, 0.3%), or fluconazole (FLC, 150 μg/ml) for cell wall and plasma membrane stress; $NaNO_2$ (100 mM) for nitrosative stress; or cadmium sulfate ($CdSO_4$, 30 μM) for protein-folding defects and heavy-metal stress. Transformants were also exposed to UV light (250–450 $\mu J/cm^2 \times 100$), elevated temperature (37°), pH (pH 7.5), and nutrient-limiting conditions [yeast nitrogen base media (YNB)]. When used, arginine and tyrosine were added at 30 mg/liter. Transformants selected in the primary screen as having a phenotype different from the WT were confirmed through a standard 1:10 serial dilution method by spotting 1.5 μl of cellular suspension on mDixon agar in the conditions that allowed their selection.

Molecular characterization of the T-DNA insertional mutants of M. furfur

Insertional mutants with a phenotype of interest were single-colony purified and grown overnight (ON) in 25 ml of liquid mDixon for genomic DNA extraction using a CTAB extraction buffer (Pitkin *et al.* 1996). To identify the insertion sites of the T-DNA in the *M. furfur* genome, inverse PCR (iPCR) was performed (Idnurm *et al.* 2004; Ianiri and Idnurm 2015). Briefly, ~2 μg of DNA were digested with the restriction enzymes *Pvu*II, *Xho*I, *Sac*II, *Apa*I, *Eco*RI (6-bp recognition site), or *Taq*I (4-bp recognition site), column purified, and eluted in 30 μl of elution buffer. Then, 8.5 μl of digested DNA were self-ligated with T4 DNA ligase (New England Biolabs, Beverly, MA) ON at 4°, and 1 μl was used as template for iPCR using primers ai76-ai77 for DNA digested with restriction enzymes that cut outside the T-DNA region, or ai076-M13F and ai077-M13R for DNA digested with restriction enzymes that cut inside the T-DNA (Idnurm *et al.* 2004). iPCR conditions were: initial denaturation at 94° for 2 min, denaturation at 94° for 30 sec, annealing at 55° for 30 sec, and extension at 72° for 2.5 min. PCR reactions were performed using ExTaq polymerase (Taqara Bio, Shiga Japan). When ExTaq was unsuccessful, we used LaTaq polymerase (Taqara Bio) suitable for highly G+C-rich regions with an annealing temperature of 55 or 60°. Amplicons were either PCR- or gel-purified, and Sanger sequenced. Sequences were subjected to basic local alignment search tool nucleotide (BLASTn) analysis against the *M. furfur* CBS14141 genome assembly available on the National Center for Biotechnology Information (NCBI) website (reported with the previous designation as JPLK23) (Wu *et al.* 2015) and against an unpublished PacBio (Pacific Biosciences) assembly. Gene boundaries and regulatory regions were determined using unpublished RNA sequencing (RNA-seq) data, which allowed us to define the accurate locations of T-DNA insertions. Retrieved *M. furfur* sequences were subjected first to BLASTx analysis against the latest genome assembly of *M. sympodialis* (Zhu *et al.* 2017) and subsequently on the *Saccharomyces* Genome Database (SGD), to identify orthologs and infer gene function. Genes were named based on orthologous genes in *Saccharomyces cerevisiae*. Gene annotation was carried out manually based on BLAST searches and with Augustus (http://bioinf.uni-greifswald.de/augustus/submission.php), using RNAseq for untranslated regions (UTRs) and introns.

For Southern blot analysis, ~2 μg genomic DNA were digested with *Sac*II (no cut sites are within the *NAT* or *NEO* cassette, thus allowing us to determine the number of T-DNA insertions), resolved on a 0.8% agarose gel in 1× Tris-acetate EDTA (TAE) buffer, transferred to a Zeta-Probe membrane, and probed with *NAT* or *NEO* cassettes labeled with [^{32}P]-dCTP. *NAT* and *NEO* cassettes were amplified from plasmids pAIM2 and pAIM6, respectively, with universal M13F and M13R primers.

RNA extraction was performed using the standard TRIzol method (Rio *et al.* 2010). RNA was treated with the TURBO DNAse enzyme (Thermo Fisher Scientific) according to the manufacturer's instructions, and quality was assessed using a NanoDrop spectrophotometer. Then, 3 μg of purified RNA were converted into cDNA via the Affinity Script QPCR cDNA synthesis kit (Agilent Technologies). cDNA synthesized without the RT/RNAse block enzyme mixture was used as a control for genomic DNA contamination. Approximately 500 pg of cDNA were used to measure the relative expression level of target genes through quantitative real-time PCR (RT-qPCR) using the Brilliant III ultrafast SYBR green QPCR mix (Agilent Technologies) in an Applied Biosystems (Foster City, CA) 7500 Real-Time PCR System. A "no-template control" was included for each target. Technical and biological triplicates were performed for each sample. Gene expression levels were normalized using the endogenous reference gene *TUB2* and determined using the comparative ΔΔCt method.

Generation of plasmids for CRIPSR/Cas9 targeted mutagenesis in M. furfur

Plasmids for targeted mutagenesis of *M. furfur CDC55* and *PDR10* through *A. tumefaciens*-mediated transformation were assembled in *S. cerevisiae* using the binary vector pGI3, as previously reported (Ianiri *et al.* 2016, 2017a,b). The *NAT* cassette was amplified from plasmid pAIM1 using primers JOHE43277 and JOHE43278. The 5′ and 3′ flanking regions for HR were amplified from the genomic DNA of *M. furfur* CBS14141, using primer pairs

JOHE45209-JOHE45210 and JOHE45211-JOHE45212 for *CDC55*, and JOHE45201-JOHE45212 and JOHE45203-JOHE45204 for *PDR10*, respectively. The PCR products and the double-digested (*Kpn*I and *Bam*HI) binary vector pGI3 were transformed into *S. cerevisiae* using lithium acetate and PEG 3750, as previously reported (Ianiri *et al.* 2016). To assess correct recombination of the newly generated plasmids, single colonies of *S. cerevisiae* transformants were screened by PCR using primers specific for the *NAT* marker (JOHE43281-JOHE43282) in combination with primers homologous to outside of the region of the plasmid pGI3 involved in the recombination event (JOHE43279-JOHE43280). Positive clones of *S. cerevisiae* were grown ON in YPD and subjected to phenol–chloroform–isoamyl alcohol (25:24:1) plasmid extraction using a previously reported protocol (Hoffman 2001). The plasmid DNA was then introduced into the *A. tumefaciens* EHA105 strain by electroporation and transformants were selected on LB + 50 μg/ml kanamycin. PCRs were performed using ExTaq and/or LATaq polymerase as described previously, except with a 1.5-min extension time.

To generate the components of the CRISPR/Cas9 system in *Malassezia*, histone H3 was identified in the *M. sympodialis* ATCC42132 genome assembly (Zhu *et al.* 2017) through BLASTp analysis using *S. cerevisiae* H3 as the query. The 813-bp upstream and 257-bp downstream regions, including the *M. sympodialis* H3 promoter and terminator (p*H3* and t*H3*), respectively, were PCR-amplified using JOHE46457-JOHE46458 and JOHE46461-JOHE46462, respectively. High-Fidelity (HF) Phusion Taq polymerase (New England Biolabs) was used with an annealing temperature of 55° for 30 sec and extension for 1 min at 72°. Primer JOHE46457 includes a chimeric region for recombination in pPZP-201BK and a multicloning site. Primers JOHE46458 and JOHE46461 include chimeric regions for recombination with JOHE46459 and JOHE46460, which were used to amplify the *CAS9* open reading frame (ORF) from plasmid pXL1-Cas9 (Fan and Lin 2018). JOHE46462 has *Sac*II and *Spe*I restriction sites, and a region for recombination with the promoter of the 5S rRNA of *M. sympodialis* used to drive expression of the single gRNA. *CAS9* amplification did not work well with HF Phusion Taq, so we used ExTaq polymerase as described above, but with fewer cycles (20 cycles) and a 4-min extension. The *M. sympodialis* ATCC42132 ribosomal cluster was identified in the latest genome assembly and annotation (Zhu *et al.* 2017) through BLASTn analysis using internal transcribed spacer (ITS) sequences from *M. sympodialis* CBS7222 (GenBank accession number NR_103583). We PCR-amplified a 674-bp region from the end of the rRNA-eukaryotic large subunit ribosomal RNA (position 612351 on chromosome 5), including the rRNA-5S ribosomal RNA gene (position 613025 on chromosome 5), using primers JOHE46463 and JOHE46464. Primer JOHE46463 has a chimeric region complementary to JOHE46462. This PCR was performed using the touchdown protocol with an initial denaturation of 94° for 5 min, followed by 24 cycles of denaturation at 94° for 30 sec, annealing at a gradient temperature of 62° for 30 sec minus 1° per cycle, and extension at 72° for 1 min. This was followed by 16 cycles of denaturation at 94° for 30 sec, annealing at 50° for 30 sec, extension at 72° for 1 min, and final extension of 72° for 5 min. The gRNA scaffold was amplified from plasmid pSDMA64 (Arras *et al.* 2016) using primers JOHE46465 and JOHE46466. JOHE46466 includes *Spe*I and *Sac*II restriction sites, six thymine residues (6T terminator), and a chimeric region for recombination in pPZP-201BK.

The specific target sequence for *CDC55* was identified using EuPaGDT (http://grna.ctegd.uga.edu/), available on FungiDB (https://fungidb.org/fungidb/). A specific target sequence for *CDC55* was added by PCR with primers JOHE46468 and JOHE46466 using the gRNA scaffold as template. Primer JOHE46468 has a chimeric region for recombination with both the 5S rRNA sequence and the gRNA scaffold, with an intervening target sequence specific for *CDC55*. We used HF Phusion Taq as reported above. All components were gel purified, and equimolar amounts of the purified amplicons were used for overlap PCR to generate the Cas9 expression cassette (p*H3- CAS9*, t*H3*) and the complete gRNA (5S rRNA promoter fused with the gene-specific gRNA scaffold). PCRs were carried out using HF Phusion Taq and the touchdown protocol as above, with the only difference being extension times of 5 and 1 min, respectively. The two resulting amplicons were cloned into the T-DNA of pPZP201BK digested with *Kpn*I and *Bam*HI through HiFi (New England Biolabs) assembly and recovered in *Escherichia coli* DH5α. We screened *E. coli* clones for recombinant plasmids by PCR using primers specific for the plasmid backbone (JOHE43279 and JOHE43280) with JOHE46458 and JOHE46463. The plasmid sequence for CRISPR/Cas9 deletion of *CDC55* (named pGI40) was confirmed by Sanger sequencing.

To generate the CRISPR/Cas9 plasmid for targeted mutagenesis of *PDR10*, the binary vector pGI40 was digested with *Spe*I to remove the *CDC55*-specific gRNA, recovered from the gel, and purified. A *PDR10*-specific target sequence designed using EuPaGDT was added to the gRNA scaffold by PCR using primers JOHE46466 and JOHE46467, which have chimeric regions for recombination with both the 5S rRNA sequence and the gRNA scaffold, with the specific target sequence for *PDR10* in between.

This amplicon and the 5S rRNA previously generated were recombined through HiFi assembly within the T-DNA of the *Spe*I-digested pGI40 plasmid, and the novel recombinant plasmids with the *PDR10*-specific gRNA (named pGI48) were identified by Sanger sequencing. This procedure is reported in Figure 4B. Recombinant plasmids were introduced into *A. tumefaciens* through electroporation.

AtMT was performed with modifications that increase transformation efficiency compared to our previous protocol used to generate insertional mutants. Briefly, *M. furfur* was grown for 2 days at 30° and the culture was diluted to OD_{600} ~1.0. The engineered *A. tumefaciens* strains with the gene deletion cassettes and the CRISPR/Cas9 expression system were grown ON, diluted to an OD_{600} ~0.1, and incubated for

4–6 hr in shaking cultures (30°) in liquid induction medium (IM) until OD_{600} reached a value of 0.6–0.8. These bacterial cellular suspensions were mixed in 1:1, 1:2, and 2:1 ratios, respectively, and added to *M. furfur* cellular suspensions at 1:2 and 1:5 ratios, respectively. These cellular suspensions were centrifuged at 5200 × *g* for 15 min, the supernatants were discarded, and ~500 μl to 1 ml of these fungal and bacterial mixes were spotted directly onto nylon membranes placed on modified IM (mIM) agar containing 200 μM acetosyringone. These were co-incubated for 5 days at room temperature (plates maintained without Parafilm), prior to transferring the dual cultures to mDixon supplemented with NAT (100 μg/ml) to select for fungal transformants and cefotaxime (350 μg/ml) to inhibit *Agrobacterium* growth.

M. furfur transformants resistant to NAT were colony purified, and subjected to phenotypic and molecular characterization. Putative mutants for the *CDC55* gene were exposed to UV light (250–300 $\mu J/cm^2 \times 100$) to identify those with impaired growth according to the results of the forward genetic screen. For molecular analysis, 23 representative NAT-resistant, UV light-sensitive transformants were subjected to phenol–chloroform–isoamyl alcohol (25:24:1) DNA extraction, and the correct replacement of the target loci was assessed by PCR. Diagnostic PCRs to identify HR events for the *CDC55* gene were carried out with primers JOHE45213 or JOHE45874 in combination with specific primers for the *NAT* gene (JOHE43281 and JOHE43282, respectively), and with primers JOHE45215 and JOHE45216 specific for the internal region of *CDC55*. To evaluate the overall rate of HR of the CRISPR/Cas9 system, a larger number of *cdc55*Δ candidate mutants were tested for sensitivity to hydroxyurea, which was found to be the stressor with the strongest phenotype. Similarly, putative *pdr10*Δ mutants were exposed to FLC (150 μg/ml) for phenotypic characterization, and transformants displaying impaired growth were subjected to DNA extraction for molecular characterization. Diagnostic PCRs were carried out using primers JOHE45205 and JOHE45206, alone and in combination with specific primers for the *NAT* gene (JOHE43281 and JOHE43282, respectively), and with primers JOHE45207 and JOHE45208 specific for the internal region of *PDR10*. PCR analyses consisted of 34 cycles of denaturation at 94° for 30 sec, annealing at 55° for 30 sec, extension at 72° of 1 min/kb with an initial denaturation at 94° for 2 min, and a final extension at 72° for 5 min. PCR analyses were performed using ExTaq (Takara) according the manufacturer's instructions. To detect HR events at the 3′ region of *CDC55* and to amplify the full-length *PDR10* gene, LATaq polymerase (Takara) with Buffer I was used. PCR for *CAS9* was carried out with ExTaq, and the touchdown protocol with primers JOHE46459–JOHE46461. PCR for the gRNA was carried out with JOHE46465 and JOHE46466 using ExTaq as reported above. All the primers used are listed in Supplemental Material, Table S1.

Phenotypic analysis of the target mutants was performed on mDixon agar by spotting 1.5 μl of 1:10 dilutions of each cellular suspension under the following conditions: UV (250–450 μJ × 100), hydroxyurea (50 mM), benomyl (50 μM), FLC (150 μg/ml), amphotericin B (AmB, 50 μg/ml), 5-flucytosine (1 mg/ml), caspofungin (100 μg/ml), cyclosporin A (CsA) at 100 μg/ml both alone and in combination with 10 mM of lithium chloride, tacrolimus (FK506) at 100 μg/ml both alone and in combination with 10 mM of lithium chloride, and dimethyl sulfoxide (40 μl), which was used to dissolve benomyl (10 mM).

Genomic comparison and phylogeny of the ABC transporter of M. furfur and M. sympodialis

The predicted amino acid sequences of *S. cerevisiae* Pdr10, Pdr5, Pdr15, Pdr12, Snq2, Pdr18, Aus1, and Pdr11 were used as queries for tBLASTn and BLASTp searches against the genomes of *M. furfur* CBS14141 and *M. sympodialis* ATCC 42132, available on GenBank (Wu *et al.* 2015; Zhu *et al.* 2017). The *Malassezia* best hits were retrieved, and the encoded proteins for *M. furfur* were predicted using Augustus (http://bioinf.uni-greifswald.de/augustus/submission.php) based on RNAseq evidence for UTRs and introns. The web portal of ACT Artemis (https://www.webact.org/WebACT/home) was used for synteny analysis of an ~15,000-bp region of *M. sympodialis* and *M. furfur*, containing orthologs of the Pdr10-encoding genes. tBLASTx analysis with a *E*-value of 0.1 was performed. For phylogeny, the aforementioned predicted ABC transporter proteins were aligned using MUSCLE and the phylogenetic tree was generated with MEGA 7 (http://www.megasoftware.net/) (Kumar *et al.* 2016), using the maximum likelihood method (LG model, five discrete γ categories) and 100 bootstrap replications.

Data availability

Strains and plasmids are available upon request. The authors affirm that all data necessary for confirming the conclusions of the article are present within the article, figures, and tables. Supplemental material available at FigShare: https://doi.org/10.25386/genetics.8309342.

Results

Molecular and phenotypic characterization of M. furfur insertional mutants

Insertional mutants of *M. furfur* were generated through AtMT using both *NAT* and *NEO* dominant drug-resistance markers. A total of 767 insertional mutants were isolated and their growth was assayed under several stress conditions (see *Materials and Methods*, and Table 1). A total of 19 mutants (~2.5%) displayed phenotypes different from the WT and were selected for further characterization.

iPCR was utilized to identify the genes inactivated by the T-DNA insertions. The sequenced amplicons were compared to the unannotated *M. furfur* CBS14141 genome assemblies (one reported in NCBI, and another unpublished based on PacBio sequencing) coupled with RNAseq data, which facilitated the identification of the coding and regulatory sequences. This allowed an accurate determination of T-DNA

Table 1 Insertional mutants for *M. furfur* isolated in the forward genetic screen

Strains	Phenotype	Hit gene	Position	Comments
1A7	UV	*CDC55*	ORF	Fourth exon
1F12	$CdSO_4$	NA	NA	NA
2A8	YNB	*ARG1*	ORF	Exon
2F4	$CdSO_4$	*SEC13-PRP43*	*SEC13*-5′ region *PRP43*-5′ region	Intergenic
2G9	FLC	NA	NA	Tandem insertion
2H11	FLC, NaCl	*ERG5/PDA1*	*ERG5*-ORF/*PDA1*-5′ region	Chromosomal rearrangement
3A1	$CdSO_4$	*JLP2/TCP1*	*JLP2*-ORF/*TCP1*-5′ region	Chromosomal rearrangement
4A10	$NaNO_2$, SDS	Uncharacterized enoyl-CoA hydratase	ORF	2 T-DNA insertions
4B1	$CdSO_4$	*MAE1*	3′-UTR	2 T-DNA insertions
5D11	FLC	NA	NA	Tandem insertion
5F1	37°C	*GPD1/INO80*	*GPD1*-5′ region/*INO80*-5′ region	Chromosomal rearrangement
5F10	NaCl	*DUG1/RPC10*	*DUG1*-3′UTR/*RPC10*-5′-UTR	Chromosomal rearrangement
6A10	FLC	*SIP5*	ORF	Altered stop codon
6B2	37°C	Uncharacterized Rho GTPase	ORF	2 T-DNA insertions
6C8	YNB	*TYR1* uncharacterized gene	ORF	Nonstandard T-DNA insertion
7D5	37°C	NA	NA	NA
7D9	FLC	*PDR10- UCB6*	*PDR10*-5′ region *UBC6*-3′ region	Intergenic
7F8	FLC	*ADY2*	3′-UTR	260 bp after the predicted stop codon
7H6	37°C	*JEN1* uncharacterized protein with RNA-binding domain	*JEN1*-5′ region uncharacterized 3′ region	Intergenic

FLC, fluconazole; NA: inverse PCR failed to identify T-DNA insertions; T-DNA, transfer DNA; YNB, yeast nitrogen base; (/), chromosomal rearrangements.

insertion sites. Southern blot analysis was performed to determine the number of T-DNA insertions, revealing that 16 transformants harbored single T-DNA insertions and three transformants had two T-DNA insertions (strains 4A10, 4B1, and 6B2) (Figure 1). In parallel, iPCR allowed the characterization of 15 T-DNA insertions (Figure 2). Six strains had T-DNA insertions within predicted ORFs, two strains had insertions within UTRs, and three strains had T-DNA insertions in intergenic regions. Of the remaining eight strains, four were suspected to have chromosomal rearrangements because the T-DNA borders were found in different locations in the *M. furfur* CBS14141 genome, and the junctions between the T-DNA and the *M. furfur* genome could not be identified in four other strains. Table 1 summarizes the results of the forward genetics approach performed in this study, and properties of the T-DNA insertions are reported in Figure 2.

Two mutants with reduced growth on YNB were identified, and analysis of the genome sequence flanking the T-DNA revealed insertions in genes involved in amino acid biosynthesis (Figure 3A). Strain 6C8 had a nonstandard T-DNA insertion that generated a deletion of ~800 bp in the *M. furfur* genome. Moreover, we were unable to identify the left border sequence from iPCR and the first nucleotides obtained mapped within the ORF of *TYR1*, which encodes a prephenate dehydrogenase involved in tyrosine biosynthesis (Mannhaupt *et al.* 1989). Conversely, the right border was within the ORF of the adjacent gene encoding an uncharacterized protein with no conserved domains that shares similarity with several other *Malassezia* species and basidiomycetes. Although addition of tyrosine did not restore the growth of strain 6C8 to the WT level (Figure 3A), YNB media supplemented with all amino acids did restore growth, suggesting that Tyr1 is involved in the biosynthesis of other amino acids. In strain 2A8, T-DNA inserted within the ORF of *ARG1*, which encodes the enzyme arginosuccinate synthetase in the arginine biosynthesis pathway (Jauniaux *et al.* 1978). Addition of L-arginine to YNB was sufficient to restore a WT phenotype, confirming that *M. furfur ARG1* is involved in arginine biosynthesis (Figure 3A).

Four insertional mutants with decreased growth at an elevated temperature (37°) were identified. Of these, only strain 7H6 had a standard T-DNA insertion, which integrated between two genes: downstream of an RNA-binding domain-containing protein and upstream of *JEN1* (Figure 3B). While the RNA-binding domain-containing protein is uncharacterized in *S. cerevisiae*, Jen1 is a plasma membrane monocarboxylate/proton symporter that transports pyruvate, acetate, lactate, and other substrates (Casal *et al.* 1999). To assess which gene was affected by the T-DNA insertion and therefore responsible for the phenotype of interest, RT-qPCR was performed. Expression levels were normalized to the *TUB2* gene of *M. furfur* WT grown at 30°. Expression of the uncharacterized gene encoding the RNA-binding domain-containing protein in strain 7H6 was ~60% lower compared to the WT, whereas expression of *JEN1* was undetectable, indicating that either or both genes could be responsible for the temperature-sensitive phenotype (Figure 3B). Other transformants that displayed a temperature-sensitive phenotype had a nonstandard T-DNA insertion pattern, and they included strains 5F1, 6B2, and 7D5 (Table 1).

Strain 1A7 showed increased sensitivity to UV light (250 and 350 $\mu J/cm^2 \times 100$) compared to WT *M. furfur* CBS14141 (Figure 3C). The T-DNA inserted into the fourth exon of the *CDC55* gene in this strain. In *S. cerevisiae*, *CDC55* encodes a regulatory subunit of PP2A. *CDC55* is involved in

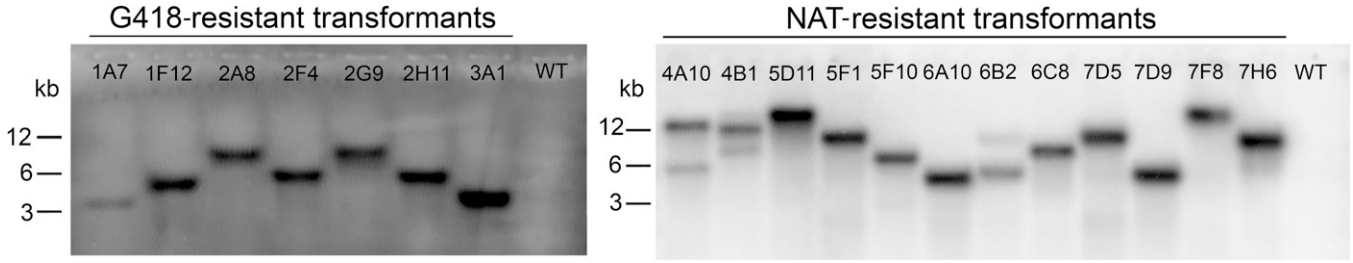

Figure 1 Southern blot analysis of *M. furfur* insertional mutants selected in the insertional genetic screen as having a phenotype different from WT. Genomic DNA was digested with *Sac*II, which does not cut within the *NAT* or *NEO* cassette, and hybridized with the ORFs of the *NEO* (left) and *NAT* (right) genes. Each hybridization band corresponds to a single T-DNA insertion. The names of the transformants and of the *M. furfur* WT are indicated. NAT, nourseothricin; NEO, G418; T-DNA, transfer DNA; WT, wild-type.

cell cycle control, and is required for successful chromosome segregation and nuclear division (Healy *et al.* 1991; Bizzari and Marston 2011).

Six strains showed increased sensitivity to the antifungal FLC (150 μg/ml) compared to the WT strain (Figure 3D). Strain 6A10 had a T-DNA insertion in the predicted stop codon of the *S. cerevisiae* ortholog *SIP5*. The function of this protein is unknown and it has no known domains. However, it has been reported to interact with both the Reg1/Glc7 phosphatase and the Snf1 kinase in response to glucose starvation (Sanz *et al.* 2000). In strain 7D9, the T-DNA was found in the intergenic region between the 5′ end of an ABC multidrug transporter gene and the 3′ end of the *UBC6* gene. As shown in Figure 6E, the closest *S. cerevisiae* homolog is the ABC transporter *PDR10*, which is the designation that we adopted. ABC multidrug transporters are involved in pleiotropic drug responses that mediate resistance to xenobiotic compounds including mutagens, fungicides, steroids, and anticancer drugs (Sipos and Kuchler 2006). *UBC6* encodes a ubiquitin-conjugating enzyme involved in ER-associated protein degradation (Walter *et al.* 2001). As confirmed by targeted mutagenesis (discussed below), the FLC-sensitive phenotype of strain 7D9 is due to T-DNA insertion in the promoter region of *PDR10*. In strain 7F8, the T-DNA inserted within the 3′-UTR of *ADY2* (Figure 3D), which encodes an ammonium and acetate transmembrane transporter involved in nitrogen utilization (Rabitsch *et al.* 2001; Paiva *et al.* 2004). For the remaining three FLC-sensitive isolates, strain 2H11 had a chromosomal rearrangement involving the *ERG5* gene and the region close to the 5′ end of the *PDA1* gene, and in strains 2G9 and 5D11, the T-DNA likely integrated in tandem repeats because iPCR amplicons consisted of both the left and right borders of the T-DNA fused together, and this prevented retrieval of the junctions between the T-DNA and the genome.

Four strains showed sensitivity to $CdSO_4$ (30 μM), and only one (strain 2F4) showed a standard T-DNA insertion in the 5′ regions of both *SEC13* and *PRP43* (Figure 3E). *SEC13* in *S. cerevisiae* encodes an essential protein that is a structural component of the coat protein complex II, of the nuclear pore outer ring, and of the Seh-1-associated complex. *S. cerevisiae PRP43* encodes an RNA helicase protein that is also essential for viability and contributes to the biogenesis of ribosomal RNA, and it is also involved in spliceosomal complex disassembly (Arenas and Abelson 1997; Giaever *et al.* 2002). RT-qPCR did not show clear downregulation of either gene (data not shown), and whether either or both genes are responsible for the cadmium sulfate-sensitive growth defect remains to be established. Because the T-DNA inserted in the 5′ region of *SEC13* and *PRP43*, whose orthologs are essential in *S. cerevisiae*, we speculate that the functions of both genes are affected or that the phenotype observed is unlinked to the T-DNA insertion. In strain 3A1, we identified a rearrangement involving the *JLP2* and *TCP1* genes, and for strain 4B1, Southern blotting indicated two T-DNA insertions, one of which was identified within the 3′-UTR of the *MAE1* gene. For strain 1F12, iPCR using different restriction enzymes was unsuccessful. We also identified a strain (4A10) that was sensitive to sodium nitrite ($NaNO_2$) and SDS. According to Southern blot analysis, strain 4A10 has two T-DNA insertions, one of which was identified in an uncharacterized enoyl-CoA hydratase gene. Another strain (5F10) was sensitive to NaCl and iPCR, and revealed the presence of a chromosomal rearrangement involving the 3′ region of the *DUG1* gene and the 5′-UTR of the *RPC10* gene.

Development of a CRISPR/Cas9 gene deletion system to generate cdc55Δ M. furfur mutants

To validate the results of the insertional mutagenesis screen, the insertional mutants 1A7 and 7D9, and their associated mutated genes, were chosen for further analysis. First, we focused on the UV-sensitive strain 1A7 with a T-DNA insertion in the *CDC55* gene. We were intrigued by this strain because *CDC55* mutation is not known to be responsible for UV sensitivity in other fungi.

To determine if the UV phenotype of the original insertional mutant in 1A7 is attributable to *CDC55* mutation, we first generated a *cdc55*Δ-targeted mutant. For targeted mutagenesis, molecular biology techniques were performed following our previously published methods (Ianiri *et al.* 2016). Regions of 1500 and 1000 bp flanking the 5′ and 3′ ends of the *CDC55* target gene, respectively, were amplified from *M. furfur* genomic DNA and fused with the *NAT* marker within the T-DNA borders of plasmid pGI3. The recombinant

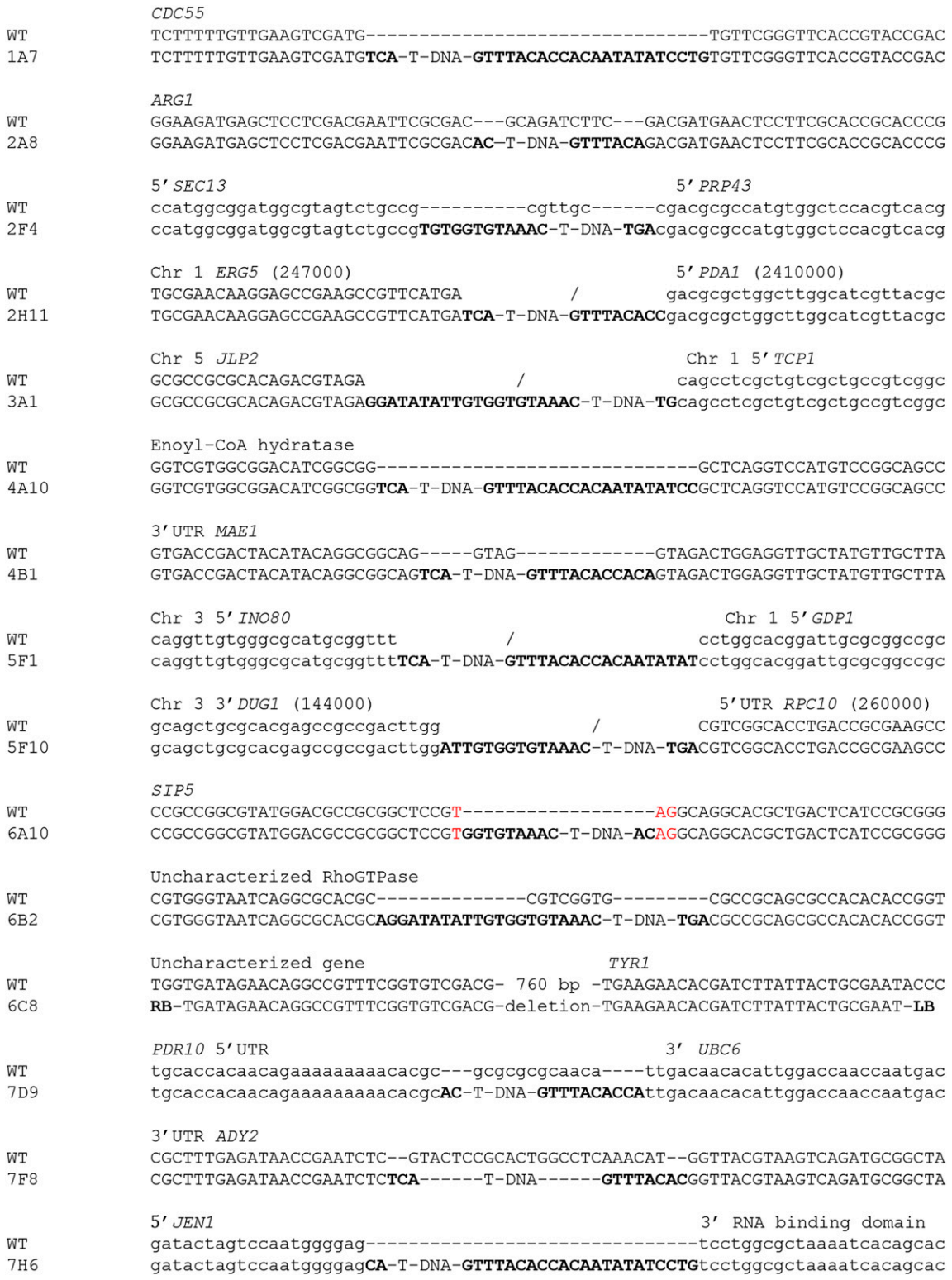

Figure 2 T-DNA insertion sites in 15 transformants of *M. furfur* as determined by iPCR. For each transformant, the mutated region and its corresponding region in the WT are shown. The region altered by the T-DNA is indicated above the sequence. When the sequences of two regions are shown above the sequence, it indicates that the T-DNA insertion involved different locations of the *M. furfur* genome. The borders of the T-DNA are depicted in bold. Uppercase letters represent nucleotides corresponding to regions with RNAseq coverage (and hence representing either 5′- or 3′-UTRs as indicated, or ORFs), while lowercase letters represent intergenic regions with no RNAseq coverage. The red nucleotides in strain 6A10 indicate a TAG stop codon. The symbol "−/−" indicates chromosomal rearrangement, with genomic locations shown in parentheses for the two transformants (2H11 and 5F10) having rearrangements involving the same chromosome. iPCR, inverse PCR; RNAseq, RNA sequencing; T-DNA, transfer DNA; WT, wild-type.

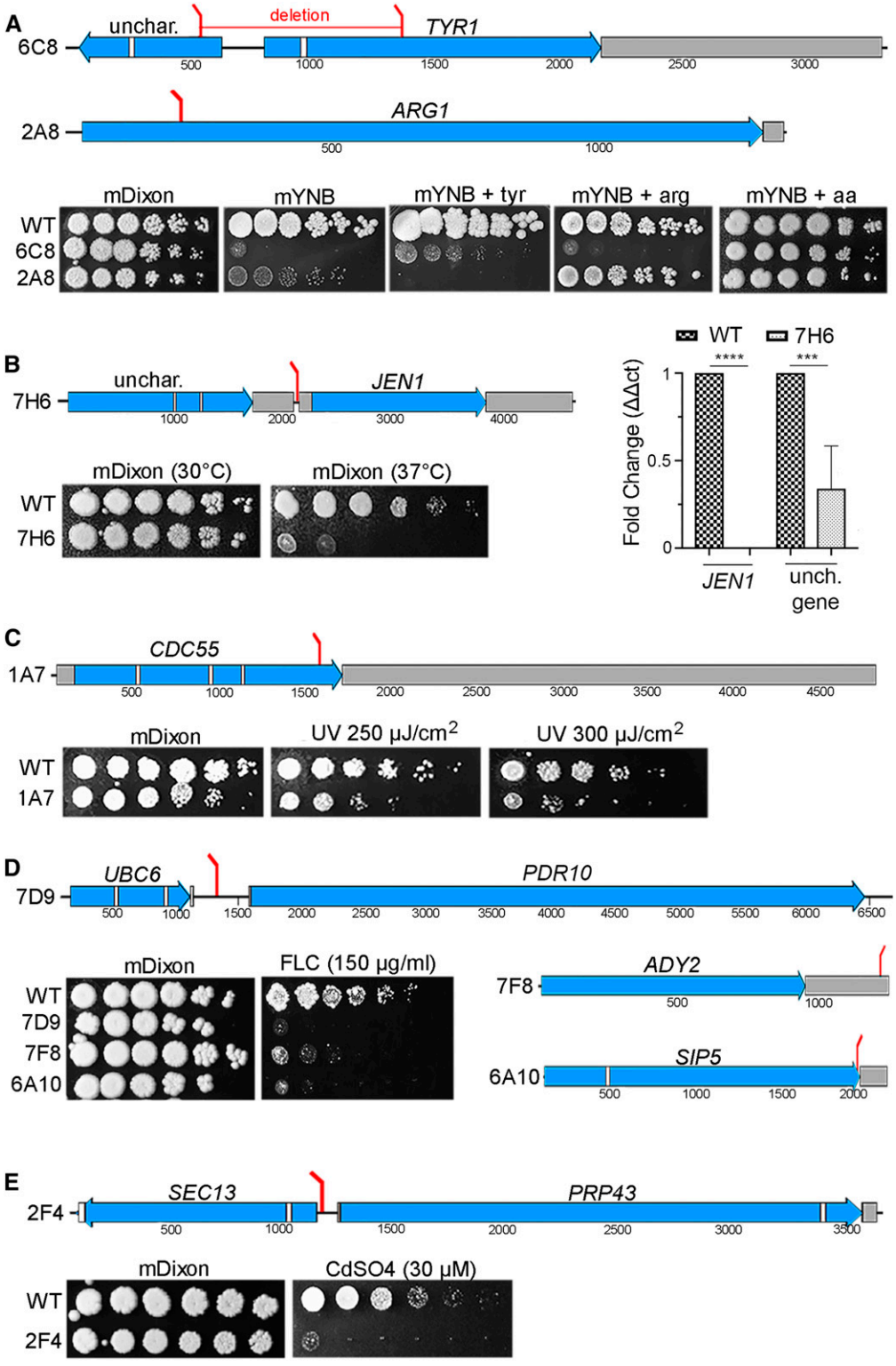

Figure 3 Position of T-DNA insertions in *M. furfur* mutants and their associated phenotypes. Each section shows mutants sensitive to the same stress or condition, such as reduced growth on mYNB medium (A), reduced growth at 37° (B), and sensitivity to UV light (C), FLC (D), or $CdSO_4$ (E). The positions of the T-DNA insertions are indicated by red bars, and in the same panel the phenotypes of the mutants are also shown. Exons are represented in blue, introns in white, and UTRs in gray. In the qPCR of (B) **** $P < 0.0001$ and *** $P < 0.001$ for each pairwise comparison. FLC, fluconazole; mDixon; modified Dixon's media; qPCR, quantitative PCR; T-DNA, transfer DNA; unch./unchar., uncharacterized; WT, wild-type; mYNB, minimal yeast nitrogen base.

plasmid (pGI41) bearing the *cdc55*Δ::*NAT* allele was identified in *S. cerevisiae* by colony PCR and transformed in *A. tumefaciens* EHA105 via electroporation. Several rounds of AtMT were performed, and NAT-resistant transformants of *M. furfur* were single-colony purified and subjected to diagnostic PCR to confirm *CDC55*-targeted mutagenesis. None of the transformants tested (0 out of > 100) showed full replacement of *CDC55*.

Next, we developed a CRISPR/Cas9 system for *M. furfur* to increase HR efficiency. Because the plasmid for targeted gene replacement of *CDC55* was already available, we generated an additional plasmid to make a DNA DSB in *CDC55*, and

then used the available *cdc55*Δ::*NAT* allele as the HDR template to repair the break. For expression of Cas9, the ORF of the *CAS9* endonuclease was cloned under the control of the strong promoter and terminator of the histone *H3* gene of *M. sympodialis* ATCC42132. To drive expression of gRNA specific for the target *CDC55* gene, the promoter of the 5S rRNA was chosen. Because the ribosomal cluster is well annotated in the newly released genome of *M. sympodialis* (Zhu *et al.* 2017), and we have evidence that *M. sympodialis* promoters and terminators are functional in *M. furfur* (Ianiri *et al.* 2016), a 689-bp region including the 5S rRNA and its upstream region was amplified from *M. sympodialis* ATCC42132. The forward primer for the p5S rRNA contained restriction sites for *Sac*II and *Spe*I to facilitate genetic manipulations. The scaffold gDNA was also obtained by PCR, and 6 thymine residues were included as a terminator. A 20-nt oligonucleotide target of gRNA was designed to match a region of the *CDC55* gene adjacent to a PAM site, and it included the 5′ and 3′ regions that overlapped with the 5S rRNA promoter and the gRNA scaffold, respectively. This target oligonucleotide was added to the gRNA scaffold through PCR as reported in Figure 4B. The five PCR fragments (p*H3*, *CAS9*, t*H3*, p5S rRNA, and gRNA) were used as templates for overlap PCRs, and two final amplicons (p*H3-CAS9-*t*H3* and p5SrRNA-gRNA) were cloned in pPZP201BK to generate plasmid pGI40 (Table 2) (Figure 4, A and B).

AtMT of *M. furfur* CBS14141 was conducted to test the developed CRISPR/Cas9 system to generate targeted gene replacement of the *CDC55* gene. Since our previous reports of AtMT of *Malassezia* (Ianiri *et al.* 2016, 2017a), we have optimized the protocol to achieve greater transformation efficiency. The main change involves the use of a 2:1 to 5:1 *Malassezia*:*A. tumefaciens* mixture that is concentrated through centrifugation before the co-incubation step on mIM (Ianiri *et al.* 2016); the detailed procedure is reported in the *Materials and Methods*. A representative subset of 23 *M. furfur* NAT-resistant transformants were single-colony purified and subjected to molecular characterization through PCR. Genotyping was performed using: (1) primers designed beyond the regions of DNA used in the generation of the deletion allele in combination with specific *NAT* primers; (2) primers internal to the gene *CDC55*; (3) primers specific for the *CAS9* genes, and (4) primers specific for the gRNA (Figure 5B). Specific amplicons of ∼1.6 and ∼1.4 kb for the 5′ (left) and 3′ (right) T-DNA-genomic DNA junctions, respectively, were obtained for all of the 23 randomly selected transformants. Accordingly, the internal region of *CDC55* was amplified only from the WT strain. No amplicons for *CAS9* or the gRNA were obtained. These results indicate that all transformants tested had full replacement of the *CDC55* gene, and an absence of *CAS9* and gRNA integration in the genome (Figure 5C). Furthermore, 64 additional random *cdc55*Δ mutant candidates were tested for sensitivity to hydroxyurea, which we found to be the most effective stressor for the *cdc55*Δ phenotype, and we found that 62 displayed impaired growth compared to WT (Figure S1). Therefore, molecular and phenotypic analyses revealed that out of 87 transformants analyzed, 85 were *cdc55*Δ mutants, resulting in a rate of successful HR of 97.7%.

In *S. cerevisiae*, *CDC55* positively regulates mitotic entry at the G2/M phase transition, mitotic spindle assembly, and the morphogenesis checkpoint, and negatively regulates mitotic exit (Wang and Burke 1997; Bizzari and Marston 2011). Null *cdc55*Δ mutants display abnormally elongated buds, decreased growth rate, and increased sensitivity to γ rays and hydroxyurea (DNA-damaging agents that interfere with DNA replication), to benomyl and nocodazole (which interfere with microtubule polymerization), and cold-induced stress. Phenotypic characterization of two representative independent *cdc55*Δ mutants confirmed that they were sensitive to UV light (Figure 5D), corroborating the phenotype of the insertional mutant 1A7. Moreover, the *cdc55*Δ mutants had slower growth rates compared to the WT strain, and increased sensitivity to hydroxyurea and benomyl (Figure 5D). Due to the inability of *M. furfur* WT to grow at low temperatures, cold sensitivity could not be determined for *M. furfur cdc55*Δ. The *cdc55*Δ mutants were subjected to microscopy analysis both under normal and stress conditions, and when exposed to hydroxyurea, the cells displayed abnormal morphology and elongated buds, similar to *S. cerevisiae cdc55*Δ mutants (Figure 5E).

Generation of a pdr10Δ M. furfur mutant with CRISPR/ Cas9

The other insertional mutant of interest was strain 7D9, which has a T-DNA insertion between the *PDR10* and *UBC6* genes, and exhibited FLC sensitivity. It was hypothesized that the phenotype of strain 7D9 was due to the T-DNA interfering with the function of *PDR10*, which is well known to mediate an antifungal drug response and therefore was chosen for targeted mutagenesis. The *pdr10*Δ::*NAT* gene disruption cassette was generated as previously described for *CDC55*, and the vector was named pGI42. For the gRNA, a primer with a specific *PDR10* target between regions that overlap with the 5S rRNA promoter and the gRNA scaffold was added to the gRNA scaffold by PCR. The resulting amplicon was then cloned together with the p5S rRNA in the T-DNA of pGI40 digested with *Spe*I, as reported in Figure 4B; this vector was named pGI48.

Cotransformation of *M. furfur* CBS14141 was performed using *A. tumefaciens* strains bearing plasmids pGI42 and pGI48, as reported in Figure 5A. Sixty *M. furfur* NAT-resistant transformants were single-colony purified and streaked onto mDixon + FLC. Five (8.3%) transformants that displayed FLC sensitivity plus a randomly selected FLC-resistant control strain were subjected to molecular characterization (Figure 6B). PCR analysis using external screening primers designed beyond the region of DNA utilized to generate the *pdr10*Δ::*NAT* deletion allele produced two amplicons: a 6183-bp amplicon for the WT and the FLC-resistant strain, and a 3933-bp amplicon for the five transformants that displayed FLC sensitivity. For these five transformants, PCR

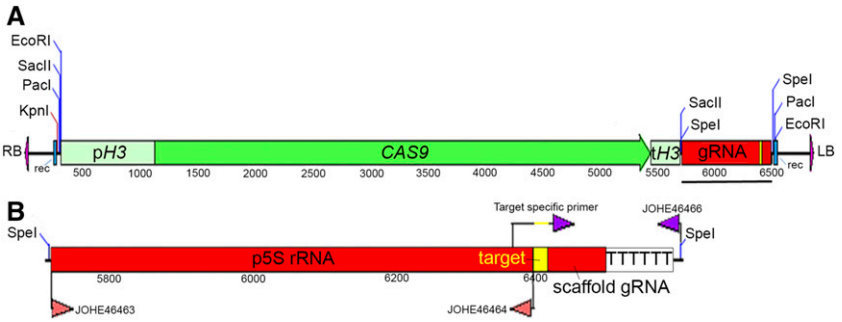

Figure 4 Development of a CRISPR/Cas9 system in *M. furfur*. (A) Complete T-DNA necessary for *CAS9* expression and gRNA excision in *M. furfur*. The promoter and terminator of the histone *H3* gene of *M. sympodialis* ATCC42132 (p*H3* and t*H3*, respectively) and the *CAS9* gene are shown in green. The gRNA is shown in red, and the gene-specific target region is shown in yellow. Sites for recombination are shown in blue, and the RB and LB of the T-DNA are shown in purple. Restriction sites were added to facilitate further molecular manipulation. The black bar indicates the full-length gRNA that is shown in greater resolution in (B). (B) The gRNA includes the 5S rRNA promoter region (p5S rRNA) obtained with primers JOHE46463 and JOHE46464 through touchdown PCR with *M. sympodialis* ATCC42132 genomic DNA. The gene-specific gRNA was obtained by PCR using a target-specific primer, which overlaps with the p5S rRNA and the gRNA scaffold, and includes a 20-nt target sequence (represented in yellow). This was used in combination with JOHE46466, which includes the 6T terminator (and a region for recombination in pPZP201BK, which is not shown). A *Spe*I restriction site was added to facilitate further use of the CRISPR/Cas9 system in *Malassezia*. To perform targeted mutagenesis of another gene, we recommend using *Spe*I digestion of the plasmid in (A) (pGI40), and cloning the two PCR products (p5S rRNA and gene-specific gRNA) through Gibson or HiFi assembly. We used this strategy to generate binary vector pGI48 for CRISPR/Cas9-mediated mutagenesis of the *PDR10* gene. CRISPR, clustered regularly interspaced short palindromic repeats; HiFi, plasmid recombination kit; gRNA, guide RNA; LB, left border; RB, right border; T-DNA, transfer DNA.

carried out using the external primers with specific *NAT* primers generated amplicons of ~1.1 and ~1.3 kb on the 5′ and 3′ regions, respectively. PCR using primers internal to the *PDR10* gene generated an amplicon of 486 bp only in the WT and the randomly selected NAT-R strain. These PCR results indicate full replacement of the *PDR10* gene in the five transformants that displayed FLC sensitivity.

Mutants of *pdr10*Δ showed hypersensitivity to FLC, indicating that the phenotype of strain 7D9 was due to T-DNA interfering with the function of *PDR10*. Because ABC transporters are involved in pleiotropic drug resistance and cellular detoxification, the phenotypic response of *pdr10*Δ mutants was tested against other antifungal drugs of clinical relevance. Surprisingly, *M. furfur pdr10*Δ mutants showed only sensitivity to FLC and grew at the WT level on AmB, 5-flucytosine, caspofungin, FK506, and CsA both alone and in combination with the plasma membrane stressor lithium chloride (Figure 6C and data not shown), which we previously showed enhances antifungal activity of tacrolimus against *M. furfur* (Ianiri *et al.* 2017a). *M. furfur pdr10*Δ mutants did not display sensitivity to the DNA-damaging agents UV or hydroxyurea, and only displayed sensitivity to the fungicide benomyl (Figure 6C).

During BLAST searches, we noted that *M. furfur* has two adjacent ABC transporter-encoding genes that are orthologs of three adjacent ABC transporter-encoding genes in *M. sympodialis* (Figure 6D), a *Malassezia* species that is a model for genomic comparison within the genus because of the high quality of its genome assembly (Zhu *et al.* 2017). Interestingly, BLASTp of these ABC transporters against *S. cerevisiae* revealed a high level of similarity (*i.e.*, *E*-value 0.0) with several ABC transporters, such as Pdr18, Pdr12, Pdr5, Pdr10, Pdr15, Aus1, and Pdr11. Reciprocal BLAST (BLASTp and tBLASTn) of these proteins against *M. furfur* and *M. sympodialis* identified only the aforementioned adjacent ABC transporters, which we named *Mf* (*M. furfur*) and *Ms* (*M. sympodialis*) *PDR10*_1, *PDR10*_2, and *PDR10*_3. The mutated gene in *M. furfur* corresponds to *PDR10*_1. Phylogenetic analysis revealed that ABC transporters of *M. furfur* and *M. sympodialis* cluster together in a maximum likelihood tree, and are related to the *S. cerevisiae* Pdr10 ABC transporter, which is the gene designation that we selected. This analysis suggests a common duplication event of the *Malassezia PDR10* (green dot on Figure 6E), followed by another more recent duplication in *M. sympodialis* (blue dot on Figure 6E).

Discussion

AtMT is considered a "silver bullet" in functional genomics of fungi, and its main applications as well as the major discoveries that it has allowed have been recently reviewed (Idnurm *et al.* 2017a). Because *A. tumefaciens* can grow under a variety of conditions, the transformation method is versatile and has been successfully applied in a number of fungi, including those with particular nutrient requirements and that are recalcitrant to other transformation approaches, such as *Malassezia* (Ianiri *et al.* 2016; Celis *et al.* 2017).

In this report, we present the first application of forward genetics in *M. furfur*, a representative species of the fungemia-causing *Malassezia* group. The goal was to generate random insertional mutants, expose them to stress to isolate strains displaying sensitivity compared to the WT, and identify the corresponding T-DNA insertion sites to determine the function of the genes causing the phenotypes. Given the lack of knowledge on gene function in *Malassezia*, insertional mutants were assayed on a variety of conditions that are known to interfere with: (1) important cellular processes, such as those involved in plasma membrane and cell wall maintenance, growth under nutrient-limiting conditions, and protein folding; (2) response to environmental stresses, such as osmotic and nitrosative stresses, UV light, elevated temperature and pH, and heavy metals; and (3) response to the antifungal FLC, which is of clinical relevance.

This loss-of-function screen allowed the characterization of eight *M. furfur* insertional mutants (1A7, 2A8, 2F4, 6A10,

Table 2 Plasmids used in the present study

Name	Background	Relevant features	Purpose	References
pAIM2	pPZP-201BK	p*ACT1-NAT*-t*ACT1*	Random insertional mutagenesis	Ianiri *et al.* (2016)
pAIM6	pPZP-201BK	p*ACT1-NEO*-t*ACT1*	Random insertional mutagenesis	Ianiri *et al.* (2016)
pPZP-201BK	NA	KAN-R	Binary vector that replicates in *E. coli* and *A. tumefaciens*	Covert *et al.* (2001)
pGI3	pPZP-201BK	Sc*URA3* + 2μ; KAN-R	Binary vector that replicates in *E. coli*, *A. tumefaciens*, and *S. cerevisiae*	Ianiri *et al.* (2017b)
pGI40	pPZP-201BK	p*H3-CAS9*-t*H3* + p5S rRNA-gRNA *CDC55*	Cas9 endonuclease and *CDC55* target gRNA	This study
pGI41	pGI3	*cdc55*::*NAT*	HDR template to generate *cdc55*Δ	This study
pGI42	pGI3	*pdr10*::*NAT*	HDR template to generate *pdr10*Δ	This study
pGI48	pGI40	p*H3-CAS9*-t*H3* + p5S rRNA-gRNA *PDR10*	Cas9 endonuclease and *PDR10_1* target gRNA	This study

HDR, homology-directed repair; KAN-R, kanamycin-resistant; gRNA, guide RNA.

6C8, 7D9, 7F8, and 7H6) that had single T-DNA insertions as determined by Southern blot analysis (Figure 1), and that displayed sensitivity to one or more stress conditions (Figure 3 and Table 1). In four strains, the T-DNA inserted within the ORFs of genes, and in one strain it was found to lie within a 3′-UTR (Figure 2, Figure 3, and Table 1), thus allowing us to define a direct link between genotype and phenotype with high confidence. Clear examples of this were *M. furfur* transformants 2A8 and 1A7. Strain 2A8 was selected because of its reduced growth on minimal medium (YNB), and it was found to have a T-DNA insertion in the *ARG1* gene. Strain 1A7 was selected for its increased sensitivity to UV light, and was found to have a T-DNA insertion in the *CDC55* gene. Two approaches were employed to validate the findings of the insertional mutagenesis screen. For strain 2A8, the addition of arginine was sufficient to rescue growth to a WT level (Figure 3A), while targeted *M. furfur cdc55*Δ mutants (Figure 5) confirmed the role of *CDC55* in UV sensitivity for strain 1A7.

In three other mutants of interest, the T-DNA inserted between two adjacent genes and further experiments were conducted to identify the gene(s) responsible for the observed phenotype. A successful approach for strain 7H6 was gene expression analysis through RT-qPCR, which revealed down-regulation of both genes flanking the T-DNA insertion (Figure 3B). Strain 7D9 was sensitive to FLC, and had a T-DNA insertion between the 3′ region of *UBC6* and the 5′ region of *PDR10*; targeted mutagenesis confirmed that the observed phenotype was due to T-DNA insertion in the promoter region of *PDR10* (Figure 6). Lastly, the RT-qPCR approach did not allow us to define which genes were responsible for the cadmium sulfate-sensitive phenotype of strain 2F4 (data not shown).

Despite the benefits of an AtMT random mutagenesis approach, analysis of the T-DNA insertion events also revealed limitations. For example, 11 of 19 *M. furfur* insertional mutants selected (∼58%) were not useful for gene function analysis due to either multiple or tandem T-DNA insertions, difficulties in identifying T-DNA insertion sites, or T-DNA insertion mediating chromosomal rearrangements (Figure 1 and Table 1). Although AtMT represents a powerful method for random mutagenesis, we and other authors have commonly found nonstandard T-DNA insertion events in the genome of both ascomycetous and basidiomycetous fungi [for more details see the following reviews and references within them (Michielse *et al.* 2005; Bourras *et al.* 2015; Idnurm *et al.* 2017a; Hooykaas *et al.* 2018)]. For example, in a recent study on systematic T-DNA insertion events in the red yeast *Rhodosporidium toruloides*, Coradetti *et al.* (2018) found that only 13% of mutants had regular T-DNA insertions and 21% of total insertions were useful to identify the mutated genes (Coradetti *et al.* 2018). Moreover, in classical forward genetic screens in which loss-of-function events are selected, it is common to isolate strains with chromosomal rearrangements that originated following the insertion of the T-DNA because these strains are generally less fit and display increased sensitivity to stress (Ianiri and Idnurm 2015). These undesirable events have been also described following AtMT of plants (Clark and Krysan 2010).

In forward genetics, the link between T-DNA insertion and phenotype is typically confirmed through: (1) sexual crosses and analysis of the phenotype in the recombinant progeny, (2) functional complementation, or (3) generation of an independent targeted mutation for the identified gene (Idnurm *et al.* 2017a). Because of the lack of a known sexual cycle in *Malassezia* and the difficulty of genetic manipulation for complementation studies, we aimed to generate *M. furfur* mutants specifically for the genes *CDC55* and *PDR10*, to validate their involvement in UV and FLC resistance, respectively. Despite several rounds of transformation, we did not obtain any *CDC55* or *PDR10* mutants. Therefore, we developed a system based on CRISPR/Cas9 to increase HR and facilitate the generation of targeted mutants in *M. furfur*. Because AtMT is the only effective transformation technique for *Malassezia*, both a functional *CAS9* cassette and a gRNA needed to be cloned within the T-DNA of a binary vector, together with a marker for selection. We also needed a specific gene replacement construct to serve as a template to repair the DSB for HR-mediated targeted mutagenesis. In fungi, CRISPR/Cas9 has been used with AtMT in two studies (Idnurm *et al.* 2017b; Kujoth *et al.* 2018). For CRISPR/Cas9 in *Malassezia*, we opted for a system that would be suitable

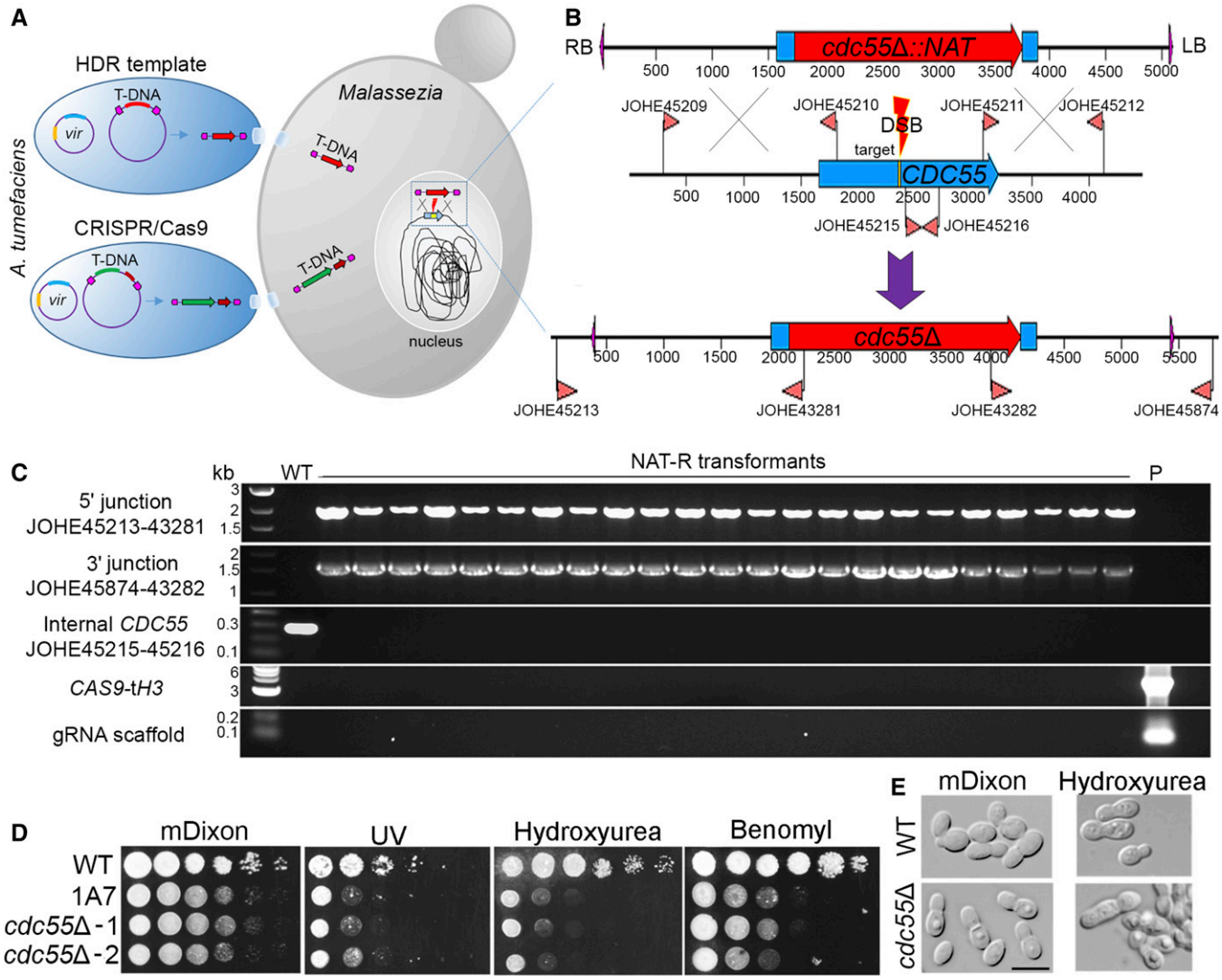

Figure 5 CRISPR/Cas9-mediated target mutagenesis of *M. furfur CDC55*. (A) Cotransformation of *M. furfur* mediated by two *A. tumefaciens* strains, one that delivers a T-DNA including the HDR template (*i.e.*, *cdc55*Δ::*NAT* deletion construct in red), and another that includes the *CAS9* cassette (in green) and the gene-specific gRNA (dark red). Also depicted are the *vir* plasmids present in *A. tumefaciens* cells that are necessary for T-DNA excision and transfer to the *M. furfur* nucleus where HR occurs. (B) Magnification of the HR event that occurs in the *M. furfur* nucleus. The top construct represents the T-DNA of the plasmid pGI41 bearing the *cdc55*Δ::*NAT* HDR template. The middle panel represents the native *M. furfur CDC55* locus, the primers used to amplify the 5′ and 3′ regions for HR, the internal primer for the *CDC55* gene, and the 20-nt target sequence (yellow). The gRNA guides Cas9 to the target site to generate a DSB that is repaired using the deletion allele as template, resulting in the targeted replacement of *CDC55* with a *NAT* dominant marker (lower panel). Primers outside the region in which HR events occur are used in combination with primers for the *NAT* marker to identify *cdc55*Δ mutants. (C) Diagnostic PCR analyses of *M. furfur* WT and NAT-resistant transformants for the identification of *cdc55*Δ mutants. Each panel used the indicated combination of primers, whose position can be found in (B). PCR primers for *CAS9* and gRNA are reported in Table S1. (D) Phenotypic analysis of *M. furfur* WT, insertional mutant 1A7, and two independent *cdc55*Δ mutants on mDixon (control), UV (300 μJ/cm^2 × 100), hydroxyurea (50 mM), and benomyl (50 μM); 1.5 μl of 10-fold serial dilutions were spotted on the agar plates, incubated at 30° for 3–7 days, and then photographed. (E) Microscopic analysis of cell morphology of WT and a representative *cdc55*Δ mutant, after growth on mDixon and mDixon supplemented with hydroxyurea (50 mM). The black bar indicates 5 μm. CRISPR, clustered regularly interspaced short palindromic repeats; DSB, double-strand break; gRNA, guide RNA; HDR, homology-directed repair; HR, homologous recombination; mDixon; modified Dixon's media; NAT, nourseothricin; T-DNA, transfer DNA; WT, wild-type.

for targeted gene replacement through HR based on cotransformation of *M. furfur* with two *A. tumefaciens* strains, one bearing the binary vector with the HDR gene deletion allele and the other with a binary vector engineered for the CRISPR/Cas9 system without a gene marker. The rationale for generating a marker-free binary vector was to: (1) have a CRISPR/Cas9 transient expression system with a reduced rate of *CAS9* and/or gRNA ectopic integration in the host genome, similar to a system developed for *C. albicans* and *C. neoformans* (Min *et al.* 2016; Fan and Lin 2018); (2) allow further genetic manipulation of the *NAT*-generated mutant using the other available *Malassezia*-specific gene marker

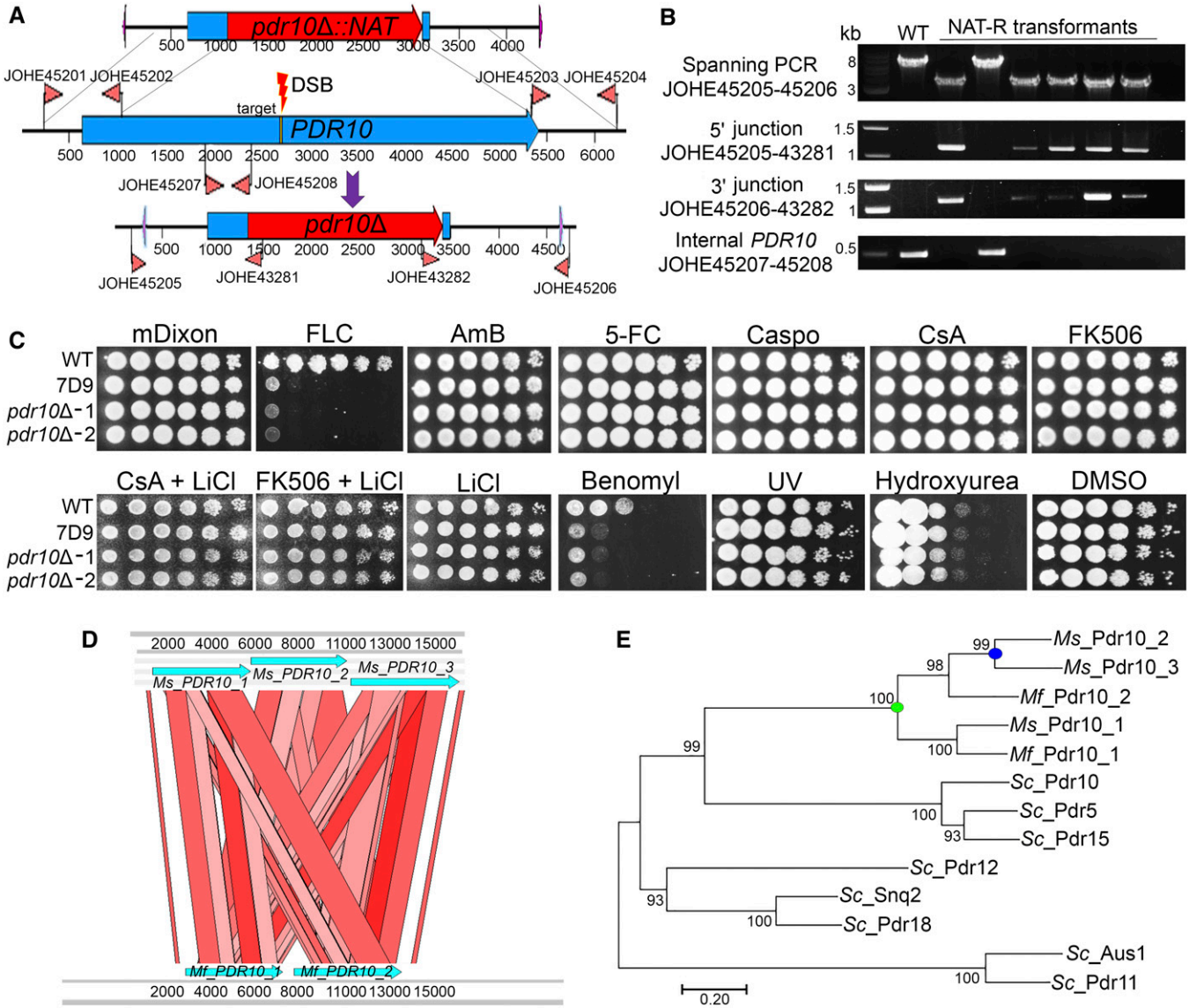

Figure 6 Targeted CRISPR/Cas9-mediated gene replacement of the *Mf PDR10* gene. (A) The T-DNA including the *pdr10*Δ::*NAT* HDR template is shown at the top. The *PDR10* gene, the primers used to amplify the 5′ and 3′ regions for HR, the internal primer for the *PDR10* gene, and the 20-nt target sequence (yellow) for the DSB are shown in the middle. The bottom part shows the *pdr10*Δ mutant allele and the primers used for PCR. (B) Diagnostic PCR analyses of *Mf* WT, and five FLC-sensitive and one FLC-resistant, transformants for the identification of *pdr10*Δ mutants. Each panel used a combination of primers that are represented in (A). (C) Cellular suspension (1.5 μl) of the WT strain CBS14141, insertional mutant 7D9, and two independent *pdr10*Δ mutants were spotted on mDixon (control), FLC (150 μg/ml), AmB (50 μg/ml), 5-FC (1 mg/ml), Caspo (100 μg/ml), CsA alone or with 10 mM of LiCl (100 μg/ml), FK506 (100 μg/ml) alone or with 10 mM of LiCl, benomyl (50 μM), UV (300 μJ/cm^2 × 100), hydroxyurea (50 mM), or DMSO [800 μl/liter (solvent used to resuspend benomyl)]. (D) ACT Artemis synteny comparison of a 15-kb region including the three copies of the *PDR10* gene of *Ms* and the two copies of the *PDR10* gene of *Mf*. (E) The predicted proteins of the *Sc* ATP-binding cassette transporters Pdr10, Pdr5, Pdr15, Pdr12, Snq2, Pdr18, Aus1, and Pdr11; *Ms* Pdr10_1, Pdr10_2, and Pdr10_3; and *Mf* Pdr10_1 and Pdr10_2 were used to generate a maximum likelihood phylogenetic tree with the LG + G method (100 bootstrap replications). AmB, amphotericin B; Caspo, caspofungin; CRISPR, clustered regularly interspaced short palindromic repeats; CsA, cyclosporine A; DSB, double-strand break; 5-FC, 5-fluorocytosine; FLC, fluconazole; G, γ category; gRNA, guide RNA; HDR, homology-directed repair; HR, homologous recombination; mDixon; modified Dixon's media; *Mf*, *M. furfur*; *Ms*, *M. sympodialis*; NAT-R, nourseothricin-resistant; *Sc*, *S. cerevisiae*; T-DNA, transfer DNA; WT, wild-type.

encoding resistance to NEO; and (3) reduce recombination within the actin promoter, and terminator regions of the *NAT* and *NEO* gene markers.

The choice of an appropriate promoter for gRNA expression has been a major challenge for the application of CRISPR/Cas9 technology in fungi. Common approaches include the use of a strong promoter recognized by RNA polymerase II, such as that of the *ACT1* or *GDP1* genes, coupled with a hammerhead ribozyme and/or hepatitis δ virus ribozyme for gRNA excision (Idnurm *et al.* 2017b; Kujoth *et al.* 2018); the use of RNA polymerase III promoters, such as the U6 promoters of small nuclear RNA used for *C. neoformans*

(Wang *et al.* 2016; Fan and Lin 2018); or the promoters of the tRNA or rRNA, with or without ribozymes (Shi *et al.* 2017). In this study, we first tested a strategy based on the use of the 5S rRNA promoter of *M. sympodialis* (Figure 4B). While we were working on developing this system, Zheng and colleagues reported a similar approach in *Aspergillus niger*, demonstrating high efficiency of gene editing using both the 5S rRNA promoter alone or in combination with the hepatitis δ virus ribozyme (Zheng *et al.* 2018). In this study, we utilized the regulatory regions of the histone *H3* gene of *M. sympodialis* to drive Cas9 expression (Figure 4A). During our first CRISPR/Cas9 attempt, we generated *M. furfur cdc55*Δ mutants with a HR rate of ~98% (Figure 4C and Figure S1), similar to the high rates observed in other studies (Fan and Lin 2018; Zheng *et al.* 2018). Given these positive results, we did not test the use of ribozymes flanking the 5S rRNA promoter. Phenotypic analysis confirmed the involvement of *CDC55* in UV resistance, and further assays revealed sensitivity of the *M. furfur cdc55*Δ mutant to benomyl and hydroxyurea (Figure 5D), which also induced abnormal bud morphology (Figure 5E). This indicates a conserved function of the cell division cycle protein Cdc55 in *M. furfur* and *S. cerevisiae*.

The CRISPR/Cas9 technology was then successfully employed for targeted mutagenesis of *PDR10*, although the rate of HR was lower for this gene, relative to *CDC55*. This could be due to several factors, such as shorter flanking regions of ~800 bp used in the HDR *pdr10*Δ::*NAT* template, the length of the *PDR10* gene (> 4 kb), the genomic location, or lower activity of the *PDR10*-specific gRNA. Analysis of *M. furfur pdr10*Δ mutants revealed an unexpected specificity of *M. furfur PDR10* for resistance to the clinically relevant drug FLC and to the antifungal agent benomyl (Figure 6C). While there are multiple studies on the pleiotropic drug-resistance function of ABC transporters in nonpathogenic (*S. cerevisiae*) and pathogenic (*C. albicans*) yeasts (Sipos and Kuchler 2006; Coste *et al.* 2008; Paul and Moye-Rowley 2014), specific analysis of Pdr10 mutation in response to several drugs has yet to be performed, and therefore it is not possible to provide a detailed comparison analysis that supports conserved or divergent functions of *PDR10* in *M. furfur*. Further bioinformatics analyses revealed that Pdr10 is the only ABC transporter present in the genome of two *Malassezia* species, and that it underwent ancestral and more recent gene duplication events (Figure 6, D and E). This suggests profound differences with other fungi, and further studies are needed to elucidate the evolution and specific roles of these *Malassezia* ABC transporters in resistance to chemicals, and their network of interactions.

Historically *Malassezia* research has been hampered by the fastidious nature, and growth and temperature requirements of species within this genus, and by their difficult identification and classification. Although understanding of *Malassezia* genetics is still limited, the T-DNA-mediated random insertional mutagenesis applied in this study coupled with a novel and efficient CRISPR/Cas9 system represent straightforward approaches to advance molecular genetics in this understudied organism. Furthermore, the available genome sequence and annotation of most *Malassezia* species, the recent introduction of animal models to study *Malassezia* interactions with the skin and the gastrointestinal tract (Limon *et al.* 2019; Sparber *et al.* 2019), and the development of molecular technologies (Ianiri *et al.* 2016, 2017a; Celis *et al.* 2017) represent key scientific advances to study the biology and pathophysiology of *Malassezia*.

Acknowledgments

We thank Tom Dawson for sharing unpublished genome and RNAseq information prior to publication, and Shelby Priest, Ci Fu, and Cecelia Wall for critical comments on the manuscript. This work was supported by National Institutes of Health/National Institute of Allergy and Infectious Diseases (NIH/NIAID) grant R01 AI50113-15 and NIH/NIAID R37 MERIT award AI39115-21 (to J.H.).

Literature Cited

Adli, M., 2018 The CRISPR tool kit for genome editing and beyond. Nat. Commun. 9: 1911. https://doi.org/10.1038/s41467-018-04252-2

Amend, A., G. Burgaud, M. Cunliffe, V. P. Edgcomb, C. L. Ettinger *et al.*, 2019 Fungi in the marine environment: open questions and unsolved problems. mBio 10: e01189-18. https://doi.org/10.1128/mBio.01189-18

Arenas, J. E., and J. N. Abelson, 1997 Prp43: an RNA helicase-like factor involved in spliceosome disassembly. Proc. Natl. Acad. Sci. USA 94: 11798–11802. https://doi.org/10.1073/pnas.94.22.11798

Arras, S. D., S. M. Chua, M. S. Wizrah, J. A. Faint, A. S. Yap *et al.*, 2016 Targeted genome editing via CRISPR in the pathogen *Cryptococcus neoformans*. PLoS One 11: e0164322. https://doi.org/10.1371/journal.pone.0164322

Bizzari, F., and A. L. Marston, 2011 Cdc55 coordinates spindle assembly and chromosome disjunction during meiosis. J. Cell Biol. 193: 1213–1228. https://doi.org/10.1083/jcb.201103076

Bourras, S., T. Rouxel, and M. Meyer, 2015 *Agrobacterium tumefaciens* gene transfer: how a plant pathogen hacks the nuclei of plant and nonplant organisms. Phytopathology 105: 1288–1301. https://doi.org/10.1094/PHYTO-12-14-0380-RVW

Byrd, A. L., Y. Belkaid, and J. A. Segre, 2018 The human skin microbiome. Nat. Rev. Microbiol. 16: 143–155. https://doi.org/10.1038/nrmicro.2017.157

Casal, M., S. Paiva, R. P. Andrade, C. Gancedo, and C. Leão, 1999 The lactate-proton symport of *Saccharomyces cerevisiae* is encoded by *JEN1*. J. Bacteriol. 181: 2620–2623.

Celis, A. M., A. M. Vos, S. Triana, C. A. Medina, N. Escobar *et al.*, 2017 Highly efficient transformation system for *Malassezia furfur* and *Malassezia pachydermatis* using *Agrobacterium tumefaciens*-mediated transformation. J. Microbiol. Methods 134: 1–6. https://doi.org/10.1016/j.mimet.2017.01.001

Cho, Y.-J., M. Park, and W. H. Jung, 2019 Resequencing the genome of *Malassezia restricta* strain KCTC 27527. Microbiol. Resour. Announc. 8: e00213-19. https://doi.org/10.1128/MRA.00213-19

Clark, K. A., and P. J. Krysan, 2010 Chromosomal translocations are a common phenomenon in *Arabidopsis thaliana* T-DNA insertion lines. Plant J. 64: 990–1001. https://doi.org/10.1111/j.1365-313X.2010.04386.x

Coradetti, S. T., D. Pinel, G. M. Geiselman, M. Ito, S. J. Mondo *et al.*, 2018 Functional genomics of lipid metabolism in the oleaginous yeast *Rhodosporidium toruloides*. eLife 7: e32110. https://doi.org/10.7554/eLife.32110

Coste, A. T., M. Ramsdale, F. Ischer, and D. Sanglard, 2008 Divergent functions of three *Candida albicans* zinc-cluster transcription factors (*CTA4*, *ASG1* and *CTF1*) complementing pleiotropic drug resistance in *Saccharomyces cerevisiae*. Microbiology 154: 1491–1501. https://doi.org/10.1099/mic.0.2007/016063-0

Covert, S. F., P. Kapoor, M.-H. Lee, A. Briley, and C. J. Nairn, 2001 *Agrobacterium tumefaciens*-mediated transformation of *Fusarium circinatum*. Mycol. Res. 105: 259–264. https://doi.org/10.1017/S0953756201003872

Cuomo, C. A., C. A. Desjardins, M. A. Bakowski, J. Goldberg, A. T. Ma *et al.*, 2012 Microsporidian genome analysis reveals evolutionary strategies for obligate intracellular growth. Genome Res. 22: 2478–2488. https://doi.org/10.1101/gr.142802.112

Dawson, T. L., 2019 *Malassezia*: the forbidden kingdom opens. Cell Host Microbe 25: 345–347. https://doi.org/10.1016/j.chom.2019.02.010

Donnarumma, G., B. Perfetto, I. Paoletti, G. Oliviero, C. Clavaud *et al.*, 2014 Analysis of the response of human keratinocytes to *Malassezia globosa* and *restricta* strains. Arch. Dermatol. Res. 306: 763–768. https://doi.org/10.1007/s00403-014-1479-1

Fan, Y., and X. Lin, 2018 Multiple applications of a transient CRISPR-Cas9 coupled with electroporation (TRACE) system in the *Cryptococcus neoformans* species complex. Genetics 208: 1357–1372. https://doi.org/10.1534/genetics.117.300656

Findley, K., J. Oh, J. Yang, S. Conlan, C. Deming *et al.*, 2013 Topographic diversity of fungal and bacterial communities in human skin. Nature 498: 367–370. https://doi.org/10.1038/nature12171

Gaitanis, G., P. Magiatis, M. Hantschke, I. D. Bassukas, and A. Velegraki, 2012 The *Malassezia* genus in skin and systemic diseases. Clin. Microbiol. Rev. 25: 106–141. https://doi.org/10.1128/CMR.00021-11

Giaever, G., A. M. Chu, L. Ni, C. Connelly, L. Riles *et al.*, 2002 Functional profiling of the *Saccharomyces cerevisiae* genome. Nature 418: 387–391. https://doi.org/10.1038/nature00935

Gioti, A., B. Nystedt, W. Li, J. Xu, A. Andersson *et al.*, 2013 Genomic insights into the atopic eczema-associated skin commensal yeast *Malassezia sympodialis*. mBio 4: e00572–e00512. https://doi.org/10.1128/mBio.00572-12

Glatz, M., P. P. Bosshard, W. Hoetzenecker, and P. Schmid-Grendelmeier, 2015 The role of *Malassezia* spp. in atopic dermatitis. J. Clin. Med. 4: 1217–1228. https://doi.org/10.3390/jcm4061217

Healy, A. M., S. Zolnierowicz, A. E. Stapleton, M. Goebl, A. A. Depaoli-Roach *et al.*, 1991 *CDC55*, a *Saccharomyces cerevisiae* gene involved in cellular morphogenesis: identification, characterization, and homology to the B subunit of mammalian type 2A protein phosphatase. Mol. Cell. Biol. 11: 5767–5780. https://doi.org/10.1128/MCB.11.11.5767

Hoffman, C. S., 2001 Preparation of yeast DNA, pp. 13.11.1–13.11.14 in *Current Protocols in Molecular Biology*, edited by F. M. Ausubel, R. Brent, R. E. Kingston, D. D. Moore, J. G. Seidman *et al*. John Wiley & Sons, New York.

Hooykaas, P. J. J., G. P. H. van Heusden, X. Niu, M. Reza Roushan, J. Soltani et al., 2018 *Agrobacterium*-mediated transformation of yeast and fungi, pp. 349–374 in *Agrobacterium Biology: From Basic Science to Biotechnology*, edited by S. B. Gelvin. Springer International Publishing, Cham. https://doi.org/10.1007/82_2018_90

Ianiri, G., and A. Idnurm, 2015 Essential gene discovery in the basidiomycete *Cryptococcus neoformans* for antifungal drug target prioritization. mBio 6: e02334-14. https://doi.org/10.1128/mBio.02334-14

Ianiri, G., A. F. Averette, J. M. Kingsbury, J. Heitman, and A. Idnurm, 2016 Gene function analysis in the ubiquitous human commensal and pathogen *Malassezia* genus. mBio 7: e01853-16. https://doi.org/10.1128/mBio.01853-16

Ianiri, G., S. Applen Clancey, S. C. Lee, and J. Heitman, 2017a FKBP12-dependent inhibition of calcineurin mediates immunosuppressive antifungal drug action in *Malassezia*. MBio 8: e01752-17 (erratum: MBio 8: e02055-17).

Ianiri, G., K. J. Boyce, and A. Idnurm, 2017b Isolation of conditional mutations in genes essential for viability of *Cryptococcus neoformans*. Curr. Genet. 63: 519–530. https://doi.org/10.1007/s00294-016-0659-2

Ianiri, G., J. Heitman, and A. Scheynius, 2018 The skin commensal yeast *Malassezia globosa* thwarts bacterial biofilms to benefit the host. J. Invest. Dermatol. 138: 1026–1029. https://doi.org/10.1016/j.jid.2018.01.008

Idnurm, A., J. L. Reedy, J. C. Nussbaum, and J. Heitman, 2004 *Cryptococcus neoformans* virulence gene discovery through insertional mutagenesis. Eukaryot. Cell 3: 420–429. https://doi.org/10.1128/EC.3.2.420-429.2004

Idnurm, A., A. M. Bailey, T. C. Cairns, C. E. Elliott, G. D. Foster *et al.*, 2017a A silver bullet in a golden age of functional genomics: the impact of *Agrobacterium*-mediated transformation of fungi. Fungal Biol. Biotechnol. 4: 6. https://doi.org/10.1186/s40694-017-0035-0

Idnurm, A., A. S. Urquhart, D. R. Vummadi, S. Chang, A. P. Van de Wouw *et al.*, 2017b Spontaneous and CRISPR/Cas9-induced mutation of the osmosensor histidine kinase of the canola pathogen *Leptosphaeria maculans*. Fungal Biol. Biotechnol. 4: 12. https://doi.org/10.1186/s40694-017-0043-0

Ishibashi, Y., T. Sugita, and A. Nishikawa, 2006 Cytokine secretion profile of human keratinocytes exposed to *Malassezia* yeasts. FEMS Immunol. Med. Microbiol. 48: 400–409. https://doi.org/10.1111/j.1574-695X.2006.00163.x

Jauniaux, J.-C., L. A. Urrestarazu, and J.-M. Wiame, 1978 Arginine metabolism in *Saccharomyces cerevisiae*: subcellular localization of the enzymes. J. Bacteriol. 133: 1096–1107.

Jinek, M., K. Chylinski, I. Fonfara, M. Hauer, J. A. Doudna *et al.*, 2012 A Programmable dual-RNA–guided DNA endonuclease in adaptive bacterial immunity. Science 337: 816–821. https://doi.org/10.1126/science.1225829

Kim, M., Y. J. Cho, M. Park, Y. Choi, S. Y. Hwang *et al.*, 2018 Genomic tandem quadruplication is associated with ketoconazole resistance in *Malassezia pachydermatis*. J. Microbiol. Biotechnol. 28: 1937–1945.

Kujoth, G. C., T. D. Sullivan, R. Merkhofer, T.-J. Lee, H. Wang *et al.*, 2018 CRISPR/Cas9-mediated gene disruption reveals the importance of zinc metabolism for fitness of the dimorphic fungal pathogen *Blastomyces dermatitidis*. mBio 9: e00412-18. https://doi.org/10.1128/mBio.00412-18

Kumar, S., G. Stecher, and K. Tamura, 2016 MEGA7: molecular evolutionary genetics analysis version 7.0 for bigger datasets. Mol. Biol. Evol. 33: 1870–1874. https://doi.org/10.1093/molbev/msw054

Li, H., B. Goh, W. K. Teh, Z. Jiang, J. P. Z. Goh *et al.*, 2018 Skin commensal *Malassezia globosa* secreted protease attenuates Staphylococcus aureus biofilm formation. J. Invest. Dermatol. 138: 1137–1145. https://doi.org/10.1016/j.jid.2017.11.034

Limon, J. J., J. Tang, D. Li, A. J. Wolf, K. S. Michelsen *et al.*, 2019 *Malassezia* is associated with Crohn's disease and exacerbates colitis in mouse models. Cell Host Microbe 25: 377–388.e6. https://doi.org/10.1016/j.chom.2019.01.007

Lorch, J. M., J. M. Palmer, K. J. Vanderwolf, K. Z. Schmidt, M. L. Verant *et al.*, 2018 *Malassezia vespertilionis* sp. nov.: a new cold-tolerant species of yeast isolated from bats. Persoonia 41: 56–70. https://doi.org/10.3767/persoonia.2018.41.04

Ma, L., Z. Chen, W. Huang da, G. Kutty, M. Ishihara *et al.*, 2016 Genome analysis of three *Pneumocystis* species reveals adaptation mechanisms to life exclusively in mammalian hosts. Nat. Commun. 7: 10740. https://doi.org/10.1038/ncomms10740

Mannhaupt, G., R. Stucka, U. Pilz, C. Schwarzlose, and H. Feldmann, 1989 Characterization of the prephenate dehydrogenase-encoding gene, *TYR1*, from *Saccharomyces cerevisiae*. Gene 85: 303–311. https://doi.org/10.1016/0378-1119(89)90422-8

McKenzie, R. A., M. D. Connole, M. R. McGinnis, and R. Lepelaar, 1984 Subcutaneous phaeohyphomycosis caused by *Moniliella suaveolens* in two cats. Vet. Pathol. 21: 582–586. https://doi.org/10.1177/030098588402100606

Michielse, C. B., P. J. Hooykaas, C. A. van den Hondel, and A. F. Ram, 2005 *Agrobacterium*-mediated transformation as a tool for functional genomics in fungi. Curr. Genet. 48: 1–17. https://doi.org/10.1007/s00294-005-0578-0

Min, K., Y. Ichikawa, C. A. Woolford, and A. P. Mitchell, 2016 *Candida albicans* gene deletion with a transient CRISPR-Cas9 system. mSphere 1: e00130-16. https://doi.org/10.1128/mSphere.00130-16

Morand, S. C., M. Bertignac, A. Iltis, I. C. R. M. Kolder, W. Pirovano *et al.*, 2019 Complete genome sequence of *Malassezia restricta* CBS 7877, an opportunist pathogen involved in dandruff and seborrheic dermatitis. Microbiol. Resour. Announc. 8: e01543-18. https://doi.org/10.1128/MRA.01543-18

Paiva, S., F. Devaux, S. Barbosa, C. Jacq, and M. Casal, 2004 Ady2p is essential for the acetate permease activity in the yeast *Saccharomyces cerevisiae*. Yeast 21: 201–210. https://doi.org/10.1002/yea.1056

Park, M., Y. J. Cho, Y. W. Lee, and W. H. Jung, 2017 Whole genome sequencing analysis of the cutaneous pathogenic yeast *Malassezia restricta* and identification of the major lipase expressed on the scalp of patients with dandruff. Mycoses 60: 188–197. https://doi.org/10.1111/myc.12586

Paul, S., and W. S. Moye-Rowley, 2014 Multidrug resistance in fungi: regulation of transporter-encoding gene expression. Front. Physiol. 5: 143. https://doi.org/10.3389/fphys.2014.00143

Pawar, S., D. Murray, W. Khalife, B. Robinson-Dunn, and M. McGinnis, 2002 Human infection caused by *Moniliella suaveolens*. Clin. Microbiol. Newsl. 24: 53–55. https://doi.org/10.1016/S0196-4399(02)80011-3

Pitkin, J. W., D. G. Panaccione, and J. D. Walton, 1996 A putative cyclic peptide efflux pump encoded by the *TOXA* gene of the plant-pathogenic fungus *Cochliobolus carbonum*. Microbiology 142: 1557–1565. https://doi.org/10.1099/13500872-142-6-1557

Rabitsch, K. P., A. Tóth, M. Gálová, A. Schleiffer, G. Schaffner *et al.*, 2001 A screen for genes required for meiosis and spore formation based on whole-genome expression. Curr. Biol. 11: 1001–1009. https://doi.org/10.1016/S0960-9822(01)00274-3

Rio, D. C., M. Ares, Jr., G. J. Hannon, and T. W. Nilsen, 2010 Purification of RNA using TRIzol (TRI reagent). Cold Spring Harb. Protoc. 2010: pdb.prot5439. https://doi.org/10.1101/pdb.prot5439

Sanz, P., K. Ludin, and M. Carlson, 2000 Sip5 interacts with both the Reg1/Glc7 protein phosphatase and the Snf1 protein kinase of *Saccharomyces cerevisiae*. Genetics 154: 99–107.

Shi, T.-Q., G.-N. Liu, R.-Y. Ji, K. Shi, P. Song *et al.*, 2017 CRISPR/Cas9-based genome editing of the filamentous fungi: the state of the art. Appl. Microbiol. Biotechnol. 101: 7435–7443. https://doi.org/10.1007/s00253-017-8497-9

Sipos, G., and K. Kuchler, 2006 Fungal ATP-binding cassette (ABC) transporters in drug resistance & detoxification. Curr. Drug Targets 7: 471–481. https://doi.org/10.2174/138945006776359403

Sparber, F., and S. LeibundGut-Landmann, 2017 Host responses to *Malassezia* spp. in the mammalian skin. Front. Immunol. 8: 1614. https://doi.org/10.3389/fimmu.2017.01614

Sparber, F., C. De Gregorio, S. Steckholzer, F. M. Ferreira, T. Dolowschiak *et al.*, 2019 The skin commensal yeast *Malassezia* triggers a type 17 response that coordinates anti-fungal immunity and exacerbates skin inflammation. Cell Host Microbe 25: 389–403.e6. https://doi.org/10.1016/j.chom.2019.02.002

Triana, S., A. González, R. A. Ohm, H. A. B. Wösten, H. de Cock *et al.*, 2015 Draft genome sequence of the animal and human pathogen *Malassezia pachydermatis* strain CBS 1879. Genome Announc. 3: e01197-15. https://doi.org/10.1128/genomeA.01197-15

Walter, J., J. Urban, C. Volkwein, and T. Sommer, 2001 Sec61p-independent degradation of the tail-anchored ER membrane protein Ubc6p. EMBO J. 20: 3124–3131. https://doi.org/10.1093/emboj/20.12.3124

Wang, Q. M., B. Theelen, M. Groenewald, F. Y. Bai, and T. Boekhout, 2014 Moniliellomycetes and Malasseziomycetes, two new classes in Ustilaginomycotina. Persoonia 33: 41–47. https://doi.org/10.3767/003158514X682313

Wang, Q. M., D. Begerow, M. Groenewald, X. Z. Liu, B. Theelen *et al.*, 2015 Multigene phylogeny and taxonomic revision of yeasts and related fungi in the Ustilaginomycotina. Stud. Mycol. 81: 55–83. https://doi.org/10.1016/j.simyco.2015.10.004

Wang, Y., and D. J. Burke, 1997 Cdc55p, the B-type regulatory subunit of protein phosphatase 2A, has multiple functions in mitosis and is required for the kinetochore/spindle checkpoint in *Saccharomyces cerevisiae*. Mol. Cell. Biol. 17: 620–626. https://doi.org/10.1128/MCB.17.2.620

Wang, Y., D. Wei, X. Zhu, J. Pan, P. Zhang *et al.*, 2016 A 'suicide' CRISPR-Cas9 system to promote gene deletion and restoration by electroporation in *Cryptococcus neoformans*. Sci. Rep. 6: 31145. https://doi.org/10.1038/srep31145

Watanabe, S., R. Kano, H. Sato, Y. Nakamura, and A. Hasegawa, 2001 The effects of *Malassezia* yeasts on cytokine production by human keratinocytes. J. Invest. Dermatol. 116: 769–773. https://doi.org/10.1046/j.1523-1747.2001.01321.x

Wrighton, K. H., 2019 *Malassezia restricta* plays CARDs in the gut. Nat. Rev. Microbiol. 17: 266–267. https://doi.org/10.1038/s41579-019-0188-3

Wu, G., H. Zhao, C. Li, M. P. Rajapakse, W. C. Wong *et al.*, 2015 Genus-wide comparative genomics of *Malassezia* delineates its phylogeny, physiology, and niche adaptation on human skin. PLoS Genet. 11: e1005614. https://doi.org/10.1371/journal.pgen.1005614

Xu, J., C. W. Saunders, P. Hu, R. A. Grant, T. Boekhout *et al.*, 2007 Dandruff-associated *Malassezia* genomes reveal convergent and divergent virulence traits shared with plant and human fungal pathogens. Proc. Natl. Acad. Sci. USA 104: 18730–18735. https://doi.org/10.1073/pnas.0706756104

Zheng, X., P. Zheng, K. Zhang, T. C. Cairns, V. Meyer *et al.*, 2018 5S rRNA promoter for guide RNA expression enabled highly efficient CRISPR/Cas9 genome editing in *Aspergillus niger*. ACS Synth. Biol. DOI: 10.1021/acssynbio.7b00456. https://doi.org/10.1021/acssynbio.7b00456

Zhu, Y., P. G. Engstrom, C. Tellgren-Roth, C. D. Baudo, J. C. Kennell *et al.*, 2017 Proteogenomics produces comprehensive and highly accurate protein-coding gene annotation in a complete genome assembly of *Malassezia sympodialis*. Nucleic Acids Res. 45: 2629–2643.

Communicating editor: A. Mitchell